EXPERIMENTAL INVESTIGATION OF THE MECHANICAL PROPERTIES OF NANOLAYERED METALS

A THESIS SUBMITTED TO
THE GRADUATE SCHOOL OF NATURAL AND APPLIED SCIENCES
OF
MIDDLE EAST TECHNICAL UNIVERSITY

BY

ALİCAN TUNCAY ALPKAYA

IN PARTIAL FULLFILLMENT OF THE REQUIREMENTS
FOR
THE DEGREE OF MASTER OF SCIENCE
IN
MECHANICAL ENGINEERING

AUGUST 2018

Approval of the thesis:

EXPERIMENTAL INVESTIGATION OF THE MECHANICAL PROPERTIES OF NANOLAYERED METALS

submitted by **ALİCAN TUNCAY ALPKAYA** in partial fulfillment of the requirements for the degree of **Master of Science in Mechanical Engineering Department, Middle East Technical University** by,

Prof. Dr. Halil Kalıpçılar
Dean, Graduate School of **Natural and Applied Sciences** _____

Prof. Dr. M. A. Sahir Arıkan
Head of Department, **Mechanical Engineering** _____

Asst. Prof. Dr. Sezer Özerinç
Supervisor, **Mechanical Engineering Dept.**, **METU** _____

Assoc. Prof. Dr. Y. Eren Kalay
Co-Supervisor, **Metallurgical and Materials Eng. Dept., METU** _____

Examining Committee Members:

Assoc. Prof. Dr. Y. Eren Kalay
Metallurgical and Materials Eng. Dept., METU _____

Asst. Prof. Dr. Sezer Özerinç
Mechanical Engineering Dept., METU _____

Asst. Prof. Dr. Hüsnü Dal
Mechanical Engineering Dept., METU _____

Asst. Prof. Dr. Kıvanç Azgın
Mechanical Engineering Dept., METU _____

Asst. Prof. Dr. Erkan KONCA
Metallurgical and Materials Eng. Dept., Atılım University _____

Date: 16 August 2018 _____

I hereby declare that all information in this document has been obtained and presented in accordance with academic rules and ethical conduct. I also declare that, as required by these rules and conduct, I have fully cited and referenced all material and results that are not original to this work.

Name, Last name: **Alican Tuncay Alpkaya**

Signature:

ABSTRACT

EXPERIMENTAL INVESTIGATION OF THE MECHANICAL PROPERTIES OF NANOLAYERED METALS

Alpkaya, Alican Tuncay
M.Sc., Department of Mechanical Engineering
Supervisor: Asst. Prof. Dr. Sezer Özerinç
Co-Supervisor: Assoc. Prof. Dr. Y. Eren Kalay

August 2018, 59 pages

Nanolayered metals are materials composed of alternating metallic layers with layer thicknesses on the order of 100 nm or smaller. These nanostructured materials exhibit higher yield strength, superior wear resistance, and better thermal stability compared to most conventional alloys. These outstanding mechanical properties make them promising for many fields including transportation, aerospace and energy industries. The relationship between the microstructure and mechanical properties of these materials should be well understood for being able to utilize them in applications. There have been many studies in the literature investigating the structure-property relationship for pure nanocrystalline metallic layers. However, the effects of alloying additions on the mechanical properties of these nanostructures are not well understood. This dissertation aims to investigate this topic through the detailed characterization of Cu/Nb nanolayers. Pure Cu / pure Nb nanolayers and alloyed $Cu_{90}Nb_{10}$ / pure Nb nanolayers were prepared in the form of thin films by magnetron sputtering on silicon substrates with layer thicknesses varying in the range 5 nm – 100 nm.

The films with a total thickness of 1 µm were characterized for their microstructure using X-ray diffraction and electron microscopy. Mechanical properties were determined by nanoindentation. Alloying additions improved the strength of Cu/Nb significantly for all layer thicknesses considered. The highest hardness of 6.98 GPa was obtained at a layer thickness of 5 nm, which is stronger than the hardest Cu/Nb nanolayer produced to date. High levels of strengthening cannot be explained by the conventional strengthening mechanisms, but it is in agreement with the recent molecular dynamics predictions of strengthening in alloyed nanocrystalline copper. This suggests that the strengthening is due to the reduction of the grain boundary energy of copper layers upon alloying. The findings provide a new path for further enhancing the strength of nanostructured materials and tailor their properties towards applications.

ÖZ

NANOKATMANLI METALLERİN MEKANİK ÖZELLİKLERİNİN DENEYSEL ARAŞTIRILMASI

Alpkaya,Alican Tuncay
Yüksek Lisans, Makina Mühendisliği Bölümü
Tez Yöneticisi: Doktor Öğretim Üyesi Sezer Özerinç
Ortak Tez Yöneticisi: Doçent Doktor Yunus Eren Kalay

Ağustos 2018, 59 sayfa

Nanokatmanlı metaller 100 nm ve daha küçük katman kalınlıklarına sahip alternatif metalik katmanlarından oluşan malzemelerdir. Bu nanoyapılı malzemeler, çoğu geleneksel alaşımlara kıyasla yüksek akma dayanımı, üstün aşınma direnci ve daha iyi ısıl kararlılık sergilerler. Bu olağanüstü mekanik özellikler, bu malzemeleri taşıma, havacılık ve enerji endüstrileri içeren birçok alan için umut vaadeden malzemeler yapar. Bu malzemelerin mikroyapı ve mekanik özellikleri arasındaki ilişkiyi, onların uygulamalarda kullanabilmeleri amacıyla iyi anlaşılmalıdır. Literatürde saf nanokristalin metalik katmanlar için yapı-özellik ilişkisini inceleyen birçok çalışma yapılmıştır. Bununla birlikte, alaşım eklemelerin bu nanoyapıların mekanik özellikleri üzerindeki etkileri iyi anlaşılmamıştır. Bu tez, bu konuyu Cu / Nb nanokatmanların detaylı karakterizasyonu ile araştırmayı amaçlamaktadır. Saf Cu / saf Nb nanokatmanlar ve alaşımlı Cu90Nb10 / saf Nb nanokatmanlar, silikon alttaş üzerine 5 nm – 100

nm aralığında değişen katman kalınlıklarına sahip ince film formunda magnetron saçtırma yöntemiyle hazırlanmıştır. Toplam 1 μm kalınlığındaki filmler, X ışını kırınımı ve elektron mikroskobu kullanılarak onların mikro yapıları için karakterize edildi. Mekanik özellikler nanobatma ile belirlendi. Alaşım eklemeler dikkate alınan tüm tabaka kalınlıkları için Cu / Nb'nin sertliğini önemli ölçüde artırdı. 5 nm katman kalınlığında en yüksek sertlik değeri 6.98 GPa olarak bulundu ki bu değer şimdiye kadar üretilen en sert nano katmanlı Cu/Nb dan daha serttir. Yüksek güçlendirme seviyeleri geleneksel güçlendirme mekanizmaları ile açıklanamaz, ancak bu alaşımlı nanokristalli bakırda güçlendirmenin yeni moleküler dinamik tahminleriyle uyum içindedir. Bu öneri güçlendirmenin alaşımlamayla bakır tabakaların tane sınırı enerjilerinin azalmasından kaynaklandığıdır. Bulgular, nanoyapılı malzemelerin gücünü daha fazla arttırmak ve özelliklerini uygulamalara göre uyarlamak için yeni bir yol sunmaktadır.

Anahtar Kelimeler: Nanokatmanlı metaller, nanokristalli malzeme, tane sınırı güçlendirmesi, ince filmler

Dedicated to My Family and My Wife

ACKNOWLEDGMENTS

Firstly, I would like to express my gratitude to my supervisor, Assist. Prof. Dr. Sezer Özerinç for his guidance, advice, support, encouragement and valuable suggestions throughout the thesis. It has been a privilege to be his student.

Secondly, I would like to thank my co-advisor Assoc. Prof. Dr. Eren Kalay for his guidance and experience-sharing especially in the XRD characterization and electron microscopy.

In addition, I am grateful to Servet Şehirli for sharing his experiences, thoughts, and dedication. I would also like to thank my friends in the Nanomechanics Laboratory for their patience and knowledge-sharing during my graduate studies. I would like to especially thank to Mohammad both for his friendship and also for discussions of the experiments and data analyses.

Finally, I would like to thank my family and my wife. I am grateful to them for providing me confidence for becoming successful and for motivating me on the challenging paths every time when I struggled.

TABLE OF CONTENTS

LIST OF TABLES

TABLES

LIST OF FIGURES

FIGURES

LIST OF SYMBOLS

σ_y	yield strength
σ_0	the yield strength of a single crystal structure
k_m	material constant
D	grain size
P	load
H	hardness
Ap	projected area
n	strain hardnening coefficient
m	Meyer's coefficient
P_E	emitted particle
P_i	incident particle
S_y	sputter yield
d	interatomic distance
λ	wavelength of the incident x-ray beam
n_d	diffraction order
hkl	crystalline plane
B	peak width
L	crystalline size
K	shape factor
h_p	the height of the pillar
h	total displacement
h_c	contact depth
h_s	displacement of the contact perimeter
S	stiffness
f_{inter}	intercept factor
E	elastic modulus

E_r	reduced elastic modulus
υ	poisson ratio
υ_i	poisson ratio of indenter material
C^0	total compliance
C_s	sample's compliance
C_f	load frame compliance
u	total displacement
u_e	displacement of elastic part
u_p	displacement of plastic part
δ_t	displacement of the flat punch
δ_s	displacement of the substrate

ABBREVIATIONS

AFM	atomic force microscopy
FEM	finite element method
FIB	focused ion beam
SEM	scanning electron microscopy
TEM	transmission electron microscopy
XRD	X-ray diffraction
FWHM	full width at half maximum
PVD	physical vapor deposition
ARB	accumulative roll bonding

CHAPTER 1

INTRODUCTION

Nanostructured metals are materials whose features such as grain boundaries, pores and interfaces have a characteristic size below 100 nm. Compared to conventional materials, these structures exhibit higher yield strength, superior wear resistance, and better thermal stability [1]. These outstanding mechanical properties make them promising materials for many fields such as space, aviation, defense, and energy sectors [2–5].

A detailed understanding of the mechanical properties of these new generation materials is crucial for the optimization of their properties, and for the application of these materials to industrial needs. This thesis aims to contribute to this understanding by investigating the mechanical properties of nanolayered metal composites.

Cu/Nb alloying materials are model materials and materials to be developed for applications that require thermal stability at high temperature and nuclear radiation resistance in the future. As it can be seen in Figure 2, Cu / Nb alloy model has thermal stability up to 800 ° C. And these structures remain stable according to microstructural and there is no amorphous and missible condition. This study also showed that layer morphology did not change but grain growth. [6]. Then, figure 1 investigates that the radiation resistance of these materials. In this study, temperature varies from room temperature to 1200 ^0C and the energies of He-ion bombardment change from 33 keV to 150 keV and ion flows per centimeter are 1.5 x 10^{17} $ions/cm^2$.

One of the most important results is that the radiation resistance of copper-niobium layered materials is very higher than pure copper.

Another important information about these materials is that the grain size decreases when the percentage of niobium increases. This relation also is known as Hall-Petch. One of the important studies on this relation is shown in figure 3. When the ratio of niobium increases from 2 percent to 10 percent, the grain size reduces from 39 nm to 17 nm. Additionally, $Cu_{90}Nb_{10}$ hardness is roughly 1.6 times higher than $Cu_{98}Nb_2$. In the first part of the introduction, an overview of the mechanisms responsible for the high strength of nanomaterials is given. Namely, grain boundary strengthening, solid solution strengthening, size effects, and nanolayered materials are discussed. In the second part, two micromechanical testing procedures called nanoindentation and micropillar compression are explained. In the last part, the physical vapor deposition method of nanomaterial synthesis is discussed.
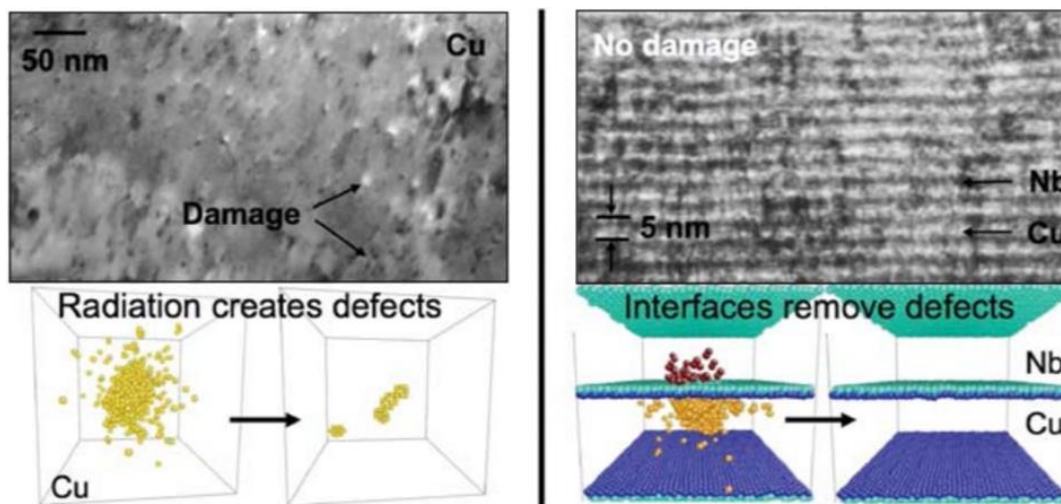
Figure 1. Transmission electron microscopy of pure copper and Cu/Nb multilayers implanted with 150 keV He to a dose of 1017 ion/cm2. The figure was taken from Demkowicz et. al. [7].
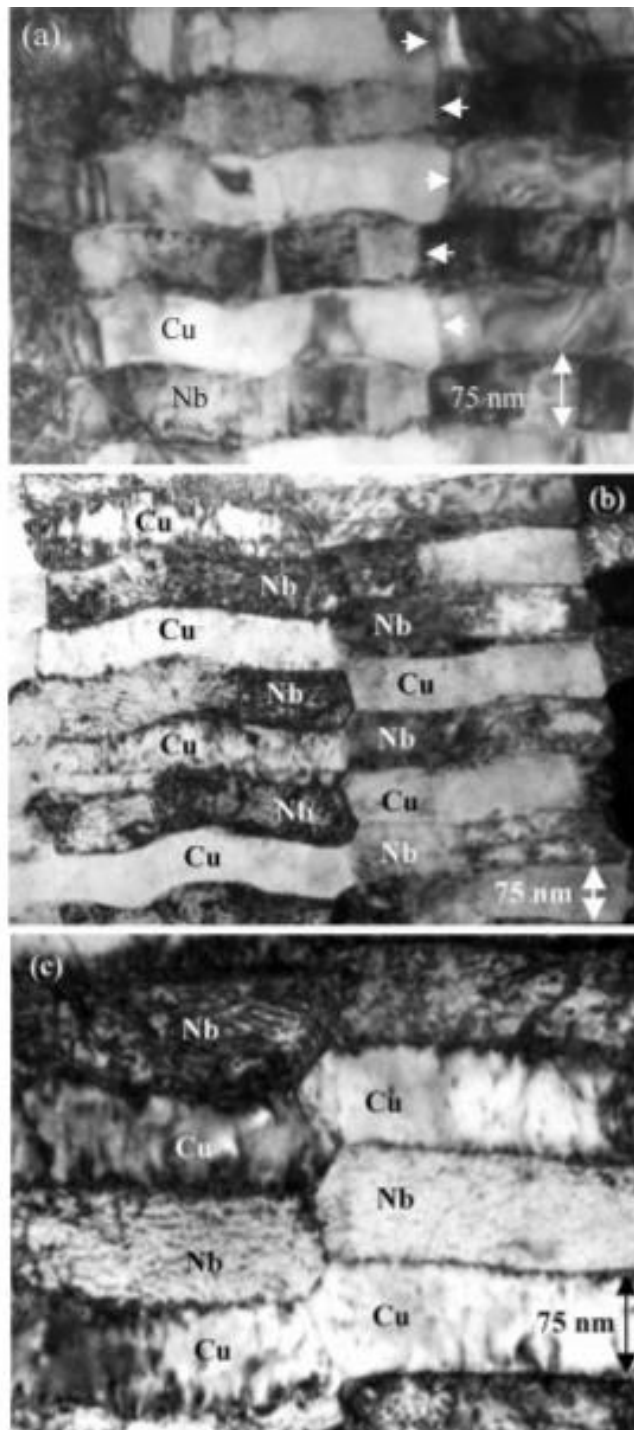
Figure 2. Thermal stability of Cu/Nb films. The figure was taken from Misra et. al. [6]
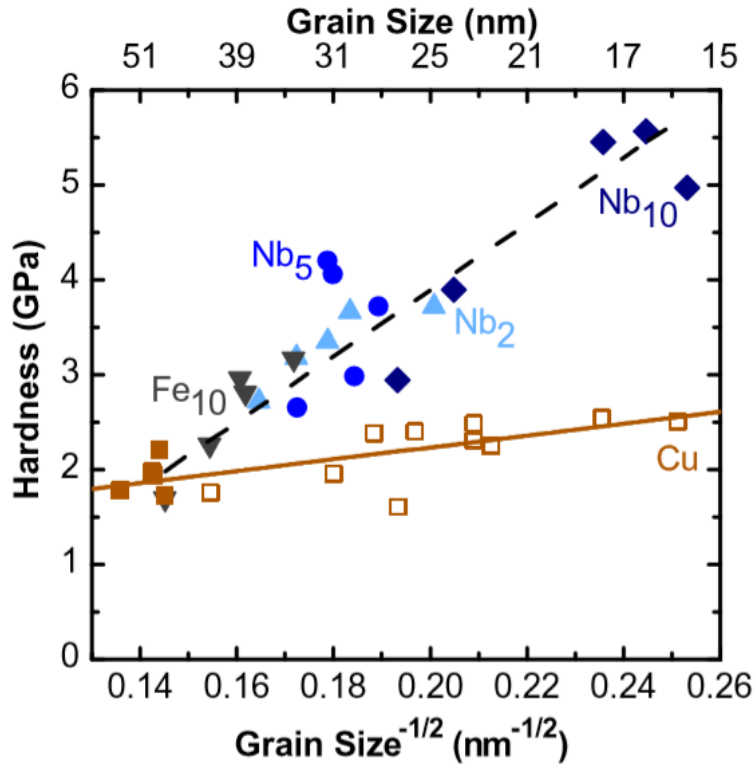
Figure 3. The relation between the grain sizes and hardness of Cu-Nb, pure Cu, and Cu-Fe (Hall-Petch Plot).The figure was taken from Ozerinc et. al. [4].

1.1. Strengthening Mechanism in Nanostructured Materials

1.1.1. Hall-Petch Strengthening

One of the most significant strengthening mechanisms in nanomaterials is Hall-Petch strengthening. This mechanism is based on a relationship between the strength and grain size [1]. As can be seen in Figure 4, the yield strength increases with decreasing grain size up to critical grain size. This critical size ranges from 10 to 50 nm. The associated equation describing this relationship is: [8–10]

$$\sigma_Y = \sigma_0 + k_m\sqrt{D} \tag{1}$$

4

where σ_Y is yield strength, σ_0 is yield strength of a single crystal, k_m is a material constant, and D is the grain size.
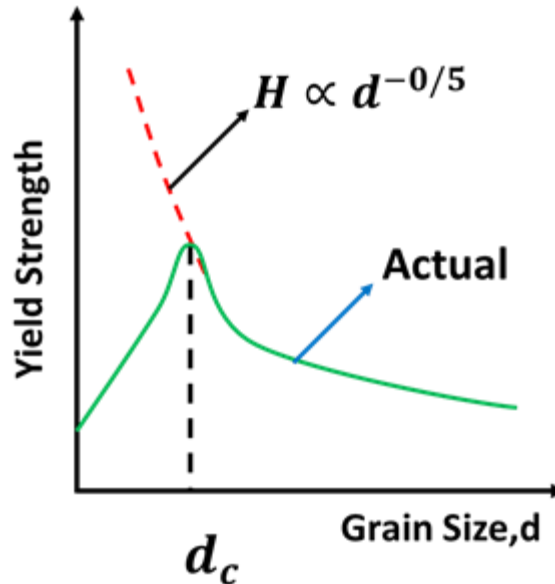
Figure 4. Schematic diagram of the Hall-Petch relationship [11] The figure is adapted from Nieh et. al. [11].

The Hall-Petch strengthening mechanism is based on the accumulation of the dislocations at the grain boundaries. Figure 5 shows that the hardness is increasing until the grain size reaches the critical grain size which is known as the theoretical point. Moreover, hardness cannot increase the hardness at that point since the grain is well-defined grain size. In other words, the grain has constant strength without any relaxation mechanism at the grain boundary. After this point, the hardness suddenly decreases, materials change the structure and they can behave as amorphous when the grains size closes zero. Therefore, the materials have not held on any strengthening effect which is also known as inverse Hall-Petch relation. In other words, yield stress decreasing with decreasing layer thickness in the regime III. The

5

main mechanism of this relation is that the grain size decreases to a critical level around 20 nm, dislocation density decreases, and eventually, a single dislocation resides in the grain. Then the dislocation accumulation at the boundary is no longer a dominant mechanism. Therefore, in this regime, a further decrease in the grain size does not lead to strengthening [11–15].
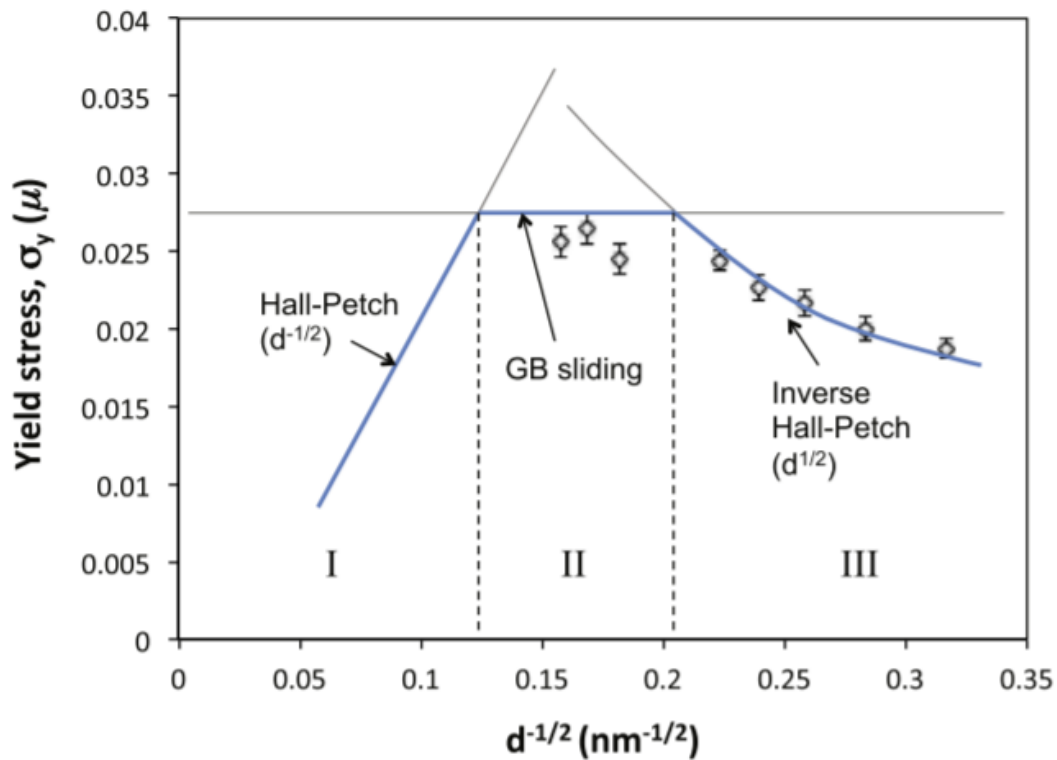
Figure 5. Grain sizes vs yield stress with different regimes. The figure was taken from Quek et. al. [14]

The layer thickness in nanolayered materials plays a similar role to that of grain boundaries [12]. In this case, decreasing layer thickness affects the strength in a similar fashion, especially for grain sizes above 100 nm. However, as the layer thickness further decreases, other mechanisms such as confined layer slip and interface crossing of dislocations start to dominate [16].

1.1.2. Solid Solution Strengthening

Solid solution strengthening is a mechanism that increases the strength of pure metals through the addition of other elements' atoms. Figure 6 illustrates the distortion of the lattice upon the addition of a substitutional solid solution. Such a distortion generates a stress field around the substitutional atom and becomes an obstacle for dislocation motion.
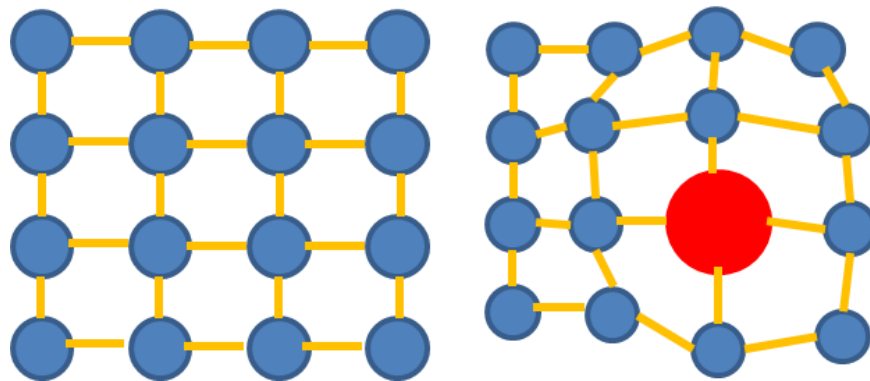
Figure 6. The schematic illustration of the substitutional solid solution and associated lattice distortion. The figure is adapted from Xu, et. al.[17].

Solid solution strengthening can become very pronounced in nanocrystalline materials. The work by Rupert et al. [5] illustrates this through the investigation of the Ni-W alloys. The results of this work are shown in Figure 7 [5]. A 40% increase in strength is observed as W content is increased from 0 to 20%. Upon the addition of W, grain size did not change much, as summarized in Table 1, and the high strength was attributed to the significant change in the shear modulus, that altered the mechanics of dislocation bowing within the nanocrystals.
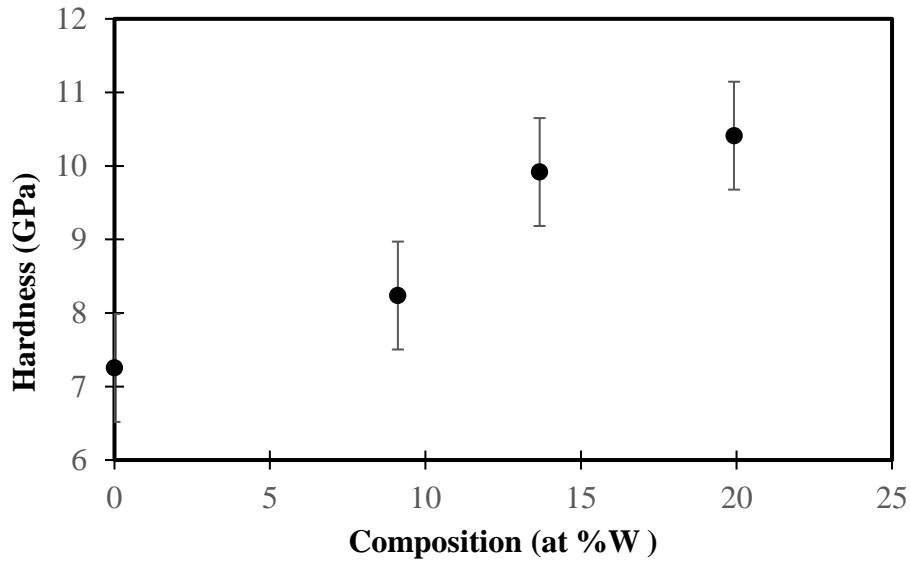
Figure 7. Increasing in hardness values of Ni–W with varying content of W [5]. The figure is adapted from Rupert et. al. [5].

Table 1. Change of hardness with respect to W additions in solid solution form [5].

W content (at.%)	Average grain size (nm)	Average hardness (GPa)
0	20	7.2
9.1	16	8.2
13.6	20	9.8
20	16	10.3

1.1.3. Size Effects

In addition to the research activities on understanding the plasticity of nanocrystalline materials, there has been important progress in understanding size effects in single crystal materials. Micropillar compression technique has enabled the researchers to probe the strength of a single crystal by varying the specimen size in the range 100 nm to 10 µm. The research activities built around this capability have suggested that there is a strong size effect in single crystals where strength dramatically increases with decreasing specimen size.

Figure 8 shows an example of a micropillar compression test, where a micropillar made of a single crystal Ni was compressed using a nanoindenter. The micropillar diameter ranged from 1 µm to 20 µm. As the diameter of the samples decreases, dislocation starvation becomes more severe due to the increased availability of free surfaces, and the level of stress required for the onset of plasticity dramatically increases.
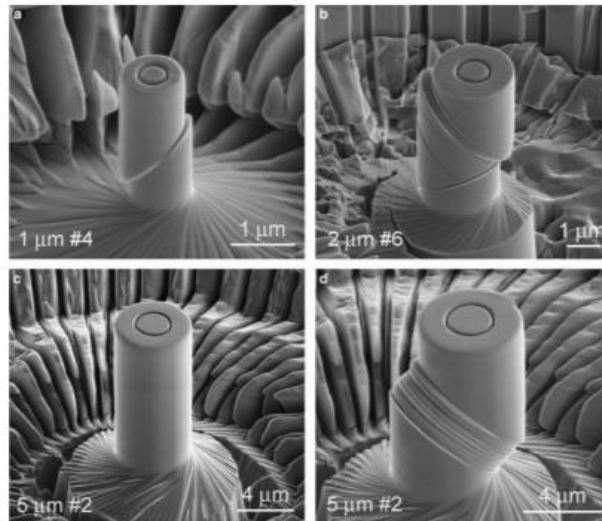
Figure 8. SEM images of micro-compression of Ni samples with diameters ranging from 1 µm to 5 µm [18]. The images were taken from Dimiduk, et. al. [18].

9

Figure 9 shows similar results for the strength of electroplated copper for varying pillar diameters. A 250 % increase in the strength is observed as the diameter was decreased from 500 nm to 111 nm. In addition, multiple strain bursts were observed in the pillars. The results demonstrate that the conventional mechanisms of plasticity are not valid at submicron sizes, and there is a great potential for generating ultra-high strength materials through the production of nanofibers and nanoporous foams and similar structures.
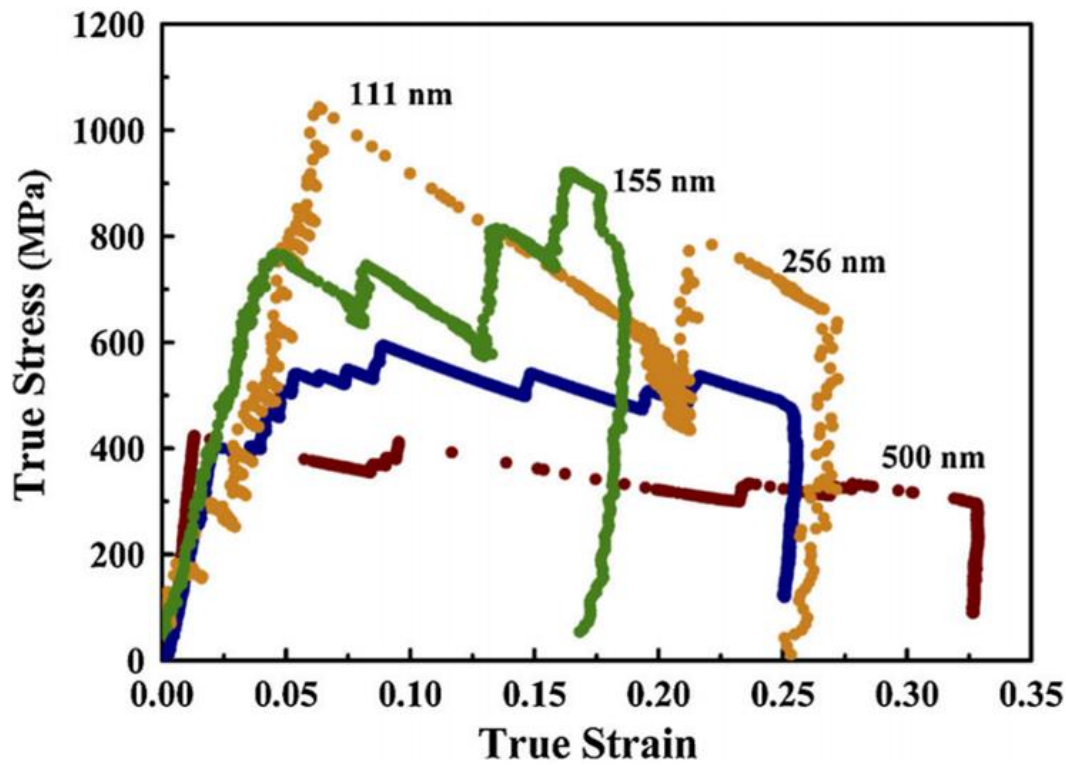
Figure 9. Representative true stress vs strain curves of the electroplated copper pillar with varying pillar diameter from 111 nm to 500 nm [19]. The figure is taken from Jennings et. al. [19].

1.1.4. Nanolayered Metals

Nanolayered metals are alternating layers of materials with layer thickness usually below 100 nm. The outstanding strength, thermal stability, and irradiation resistance make these materials promising model systems to understand and develop new generation materials for engineering applications [20]. There has been a considerable amount of work in the literature on the promising properties of Cu/Nb metallic nanolayered materials, which is also the main focus of this thesis.

Figure 10 shows that Cu/Nb strength increases with decreasing layers thickness for nanolaminates prepared by two different production methods. For the Cu/Nb produced by accumulative roll bonding (ARB) with a layer thickness of 7 nm, the hardness value reaches a maximum. This value is almost two times higher than that of 100 nm nanolayers. Even higher hardness was measured for Cu/Nb produced by physical vapor deposition (PVD). When PVD Cu/Nb metallic materials layer thickness is roughly 1.3 nm, the hardness value reaches a maximum [21].
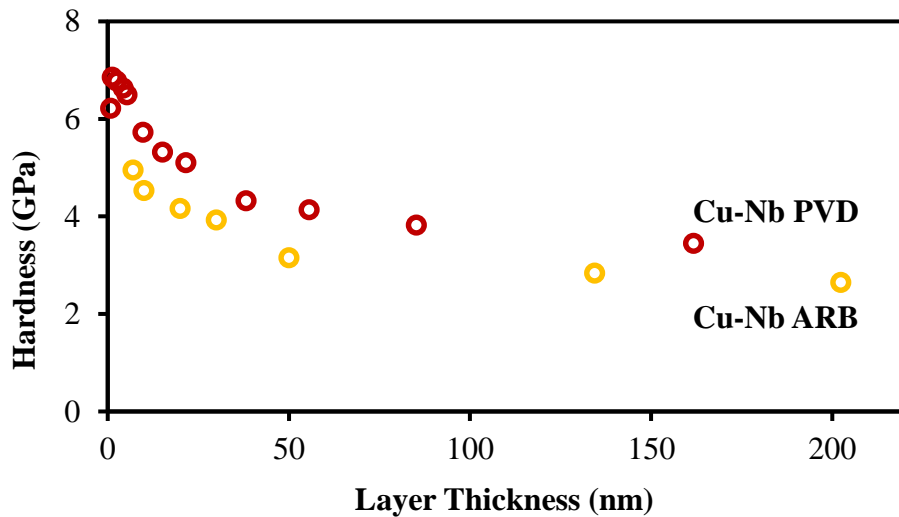
Figure 10. The hardness of multilayers of Cu/Nb produced by Physical Vapor Deposition (PVD) and Accumulative Roll Bonding (ARB) as a function of layer thickness [22].

11

Figure 11 shows three different groups of nanolayered materials [23]. The black and red symbols correspond to the bulk strength of the constituents whereas the blue marker shows the peak strength achieved by the nanolayers of these metallic pairs. Group 1 nanolaminated materials consist of metal-metal layers, Group 2 nanolaminated materials consist of metal-ceramic layers, and Group 3 is crystalline metal-metallic glass layers. This thesis focuses on Group 1, where the strength of the nanolayers is stronger than both of the constituent layers.
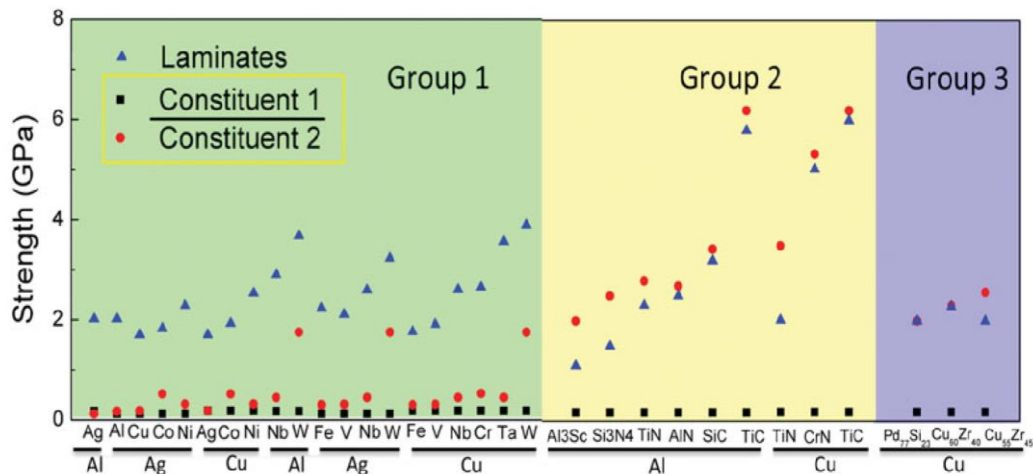
Figure 11. The strength of nanolayered materials for different combinations of constituent elements and phases [23]. This figure is taken from Wang et. al. [23].

1.2. Micromechanical Testing Techniques

Micromechanical testing is commonly used to characterize nanomaterials, thin film coatings and many other new generation materials for the determination of hardness, elastic modulus, toughness, yield strength, ultimate tensile strength and other mechanical properties [24].

The developments in sensors and actuators in the last three decades have enabled the precise measurement of force and displacement with nN and nm resolution. These advances have resulted in the development of advanced micromechanical testing techniques such as nanoindentation and micropillar compression, which are reviewed below.

1.2.1. Nanoindentation

One of the most popular micromechanical measurement technique is nanoindentation [25,26]. In the indentation test, a diamond tip penetrates the specimen surface while the displacement into the surface and the load on the sample are simultaneously measured. The characteristic load-displacement curve for a ductile material is represented in Figure 12 [25].
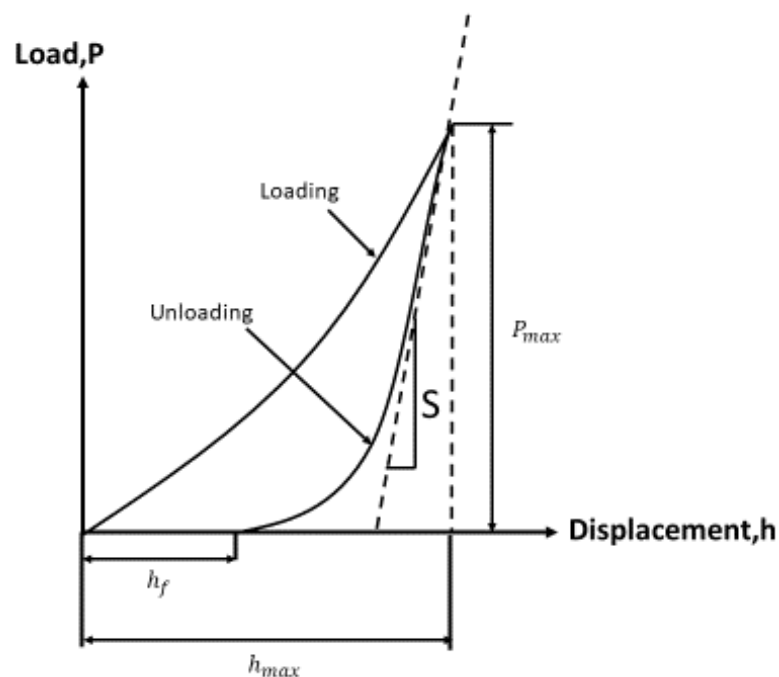
Figure 12. The schematic of a load-displacement curve for indentation[25]. The figure is taken from Oliver et. al. [25].

In figure 12, P_{max} is the peak indentation load, h_{max} is the maximum displacement when the load is at its peak, h_f is the final depth after unloading and S is the stiffness of the initial part of the unloading.

Hardness is defined as,

$$H = \frac{P_{max}}{A_p}$$ (2)

where H is the hardness, P is the peak load, and A_p is the projected area of the contact surface between the tip and the sample. P is directly measured while A_p is not a measured quantity and it should be determined after the test. While by virtue of combined plastic and elastic deformation mechanisms, the loading part can be complex to interpret, the unloading part primarily consists of elastic recovery. As a result, the unloading cycle is more suitable for estimating the contact area at the peak load. For the determination of A_p, the Oliver-Pharr method is commonly employed [25].

Nanoindentation has many advantages such as simple sample preparation, well-established data analysis and the application of multiple tests in a small area with high speed. However, nanoindentation cannot directly measure the yield strength of the material, which is a more relevant parameter from an engineering perspective. Nevertheless, one can estimate the yield strength of a material from its hardness [27]. This relation is defined by:

$$\sigma_y = \frac{H}{3}(0.1)^n$$ (3)

14

where n is the strain hardening coefficient which is obtained from Meyer's coefficient, m, using by relation $n = m\text{-}2$ and σ_y is the yield strength.

Substrate effects, pile-up, and sink-in effects are the primary limitations of nanoindentation [28]. A substrate with significantly different properties when compared to the film being tested can alter the measurement results. To minimize the error, the indentation depth should not exceed 10% of the film thickness [28–32]. On the other hand, pile-up by the side of the indenter tip can result in an error in the hardness calculation due to the error in the contact area estimation. Another problem is the contact stiffness uncertainty due to the creep of the specimen. Since creep affects the unloading stiffness, after the loading period, the load should be held constant for about ten seconds, before unloading starts [28].

1.2.2. Micropillar Compression

As discussed in the previous section, the nanoindentation method is an effective and common method to obtain various mechanical properties. However, the main disadvantage of the method is that hardness is not a fundamental mechanical property such as yield strength. A new method has recently been developed enabling the direct measurement of the yield stress and elastic modulus at the microscale [33]. This technique is known as the micropillar compression method. In this approach, a microcylindrical specimen is fabricated and a nanoindenter equipped with a flat punch compresses the specimen. Load and displacement are measured, which can be converted to stress-strain behavior, analogous to conventional compression experiments.

One of the most commonly used fabrication methods for micropillar samples utilizes a focused ion beam. The range of the pillar diameters that can be prepared by this technique approximately varies from 20 μm down to 100 nm. [34]. This method is used in this thesis and will be further detailed in Chapter 2.

Figure 13 shows the true stress-true strain data of a micropillar compression experiment for Cu/Nb nanolayered materials. When the layer thickness is 5 nm, the flow stress reaches a maximum of 2.4 GPa. This stress is about 30 percent greater than the sample with a 40 nm layer thickness. One of the most important reasons for the higher strength is grain boundary strengthening.
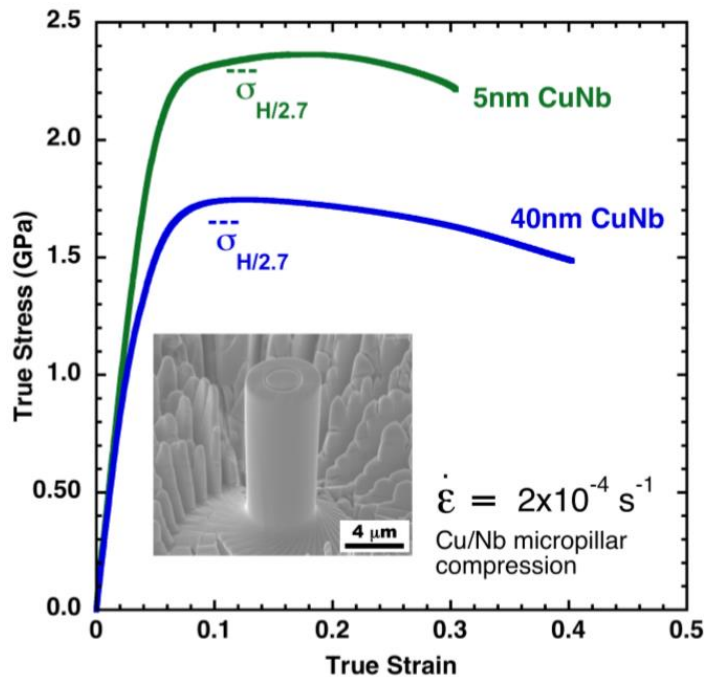
Figure 13. True stress vs. true strain curve for Cu/Nb micropillar with layer thickness at 5 nm and 40 nm [35]. The figure is taken from Mara et. al. [35].

1.3. Physical Vapor Deposition

Physical vapor deposition is an effective technique for preparing nanostructured materials in the form of a coating in a vacuum environment. The process is applied by evaporating the solid target material onto a substrate.

Among the PVD techniques, one of the most commonly used ones is sputtering. In this technique, target atoms are sputtered from the target surface via the inert gas plasma (usually Ar^+). As it can be seen in Figure 14 [36], argon ions accelerate towards the target surface, and they knock target atoms out. Then, the sputtering ions get accelerated towards the substrate by the magnetic field. The disadvantage of this process is the low deposition rate and high heating effect on the substrate [37]. The accelerated ions hitting on the surface generate secondary electrons sustaining the plasma through the chamber. These secondary electrons cause excessive heating on the substrate.
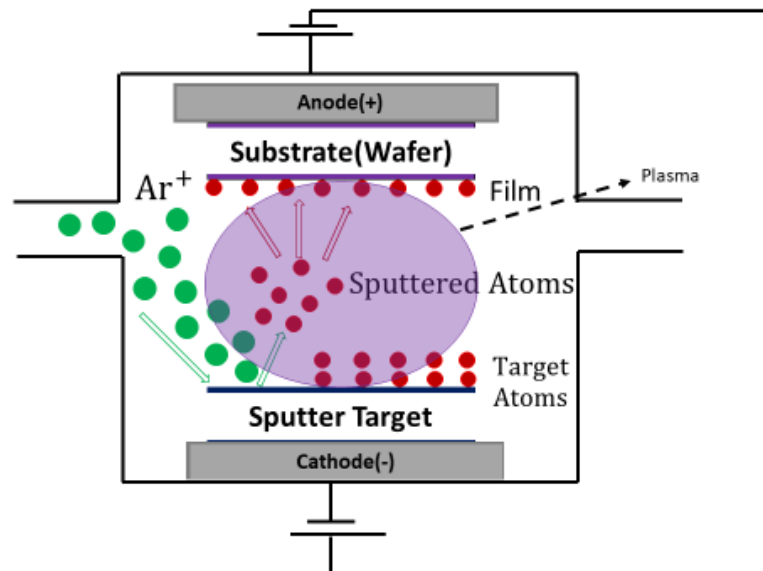
Figure 14. Schematic of DC sputtering mechanism [36]. The figure is taken from Mattox [36].

On the contrary to classical sputtering, the magnetic field is positioned parallel to the target surface in the *magnetron sputtering*, as it can be seen in Figure 15. This positioned magnetic field enables the prevention of the propagation of the secondary electrons towards the substrate. Consequently, the secondary electrons do not hit the

substrate, and heating is reduced. Nevertheless, for sputtering processes exceeding a couple of minutes, water cooling or an efficient conduction path is necessary.
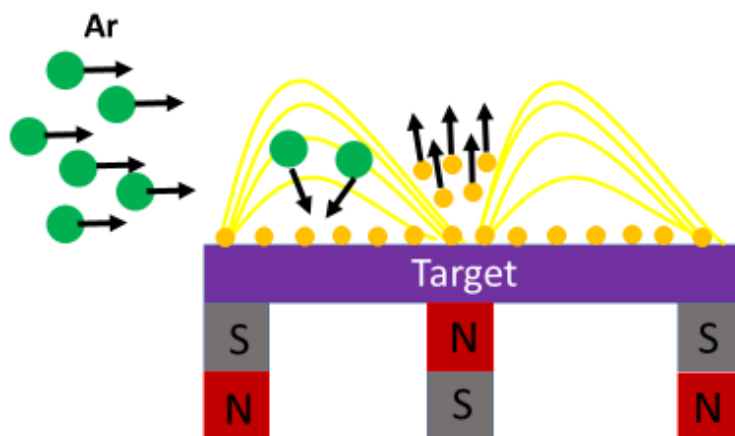
Figure 15. The schematic of the magnetron sputtering approach.

Magnetron sputtering has become an efficient and widely utilized way of generating nanostructures and nanocrystalline metallic films. In this thesis, magnetron sputtering was employed to prepare the specimens, and further details are provided in Chapter 2.

1.4. Dissertation Overview

There have been many studies regarding the mechanical properties of the copper-niobium system recently [3,4,12,23,35,38]. However, solid solution strengthening effects of these layers are currently unknown. This dissertation aims to investigate solid solution strengthening effects in copper-niobium nanolayers. This investigation is done by the addition of 10 at % niobium to copper layers, and by keeping the other parameters the same to the possible extent. The samples were prepared by magnetron

sputtering and characterized by nanoindentation, X-ray diffraction, and electron microscopy.

Chapter 2 describes the experimental procedures performed together with some principles and basics of testing methods. These include magnetron sputtering, nanoindentation, micropillar compression, X-ray diffraction, and electron microscopy.

Chapter 3 presents the results of mechanical testing through micropillar compression and nanoindentation. Results of these tests are compared with literature and discussed based on existing strengthening mechanisms.

Chapter 4 presents the preliminary results of micropillar compression and future studies to be conducted are summarized.

CHAPTER 2

EXPERIMENTAL PROCEDURE

2.1. Sample Preparation

In this section, general information about the sputter system and the coating process is given. Figure 16 shows the magnetron sputtering system used in the studies. The system is located in the Nanomechanics Laboratory of Middle East Technical University. This device was used to generate all thin films used in this thesis. The magnetron sputtering system houses two sputtering guns, one is powered by radio frequency (RF), while the other is powered by direct current (DC).
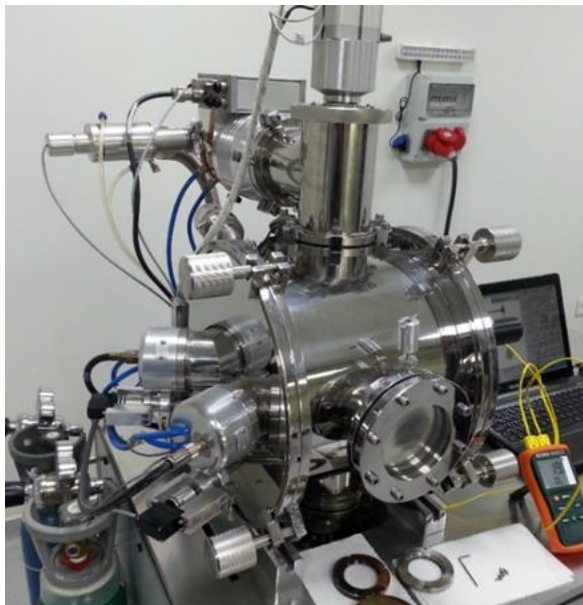
Figure 16. The image of the magnetron sputtering system.

Thin films were coated on oxidized single crystal Si wafers. 10 cm diameter prime grade wafers are cut with a diamond pen to the desired sizes similar to a standard glass slide, and it is cleaned by ultrasonication with acetone and isopropyl alcohol followed by drying with nitrogen. Prepared sample was taken into the chamber and the chamber was pumped down overnight.

For coatings of pure nanocrystalline copper layers, power was adjusted to 100 W RF. The coating duration was linearly related to the coating thickness. For pure niobium layers, the other sputtering gun was run with DC power adjusted to 100 W. For the alloyed copper coating ($Cu_{90}Nb_{10}$), RF power on the copper loaded gun was 100 W, DC power on the niobium loaded gun was adjusted to 19 W. In this process of alloy coating these two powers were used simultaneously. The purity of the target materials to be coated is 99.99 percent, all sputtering targets were taken from Lesker, their diameters were 2 inches, and thickness was 0.125 inches.

When preparing the coatings, first we open the shutter of the material to be coated, then close the shutter and open the shutter of the other target material. For Cu / Nb, we first start the copper shutter, multiply the time depending on the layer thickness to be coated with the previously determined rate and start the process. Then the copper shutter is closed and the niobium shutter is opened and the time is determined by multiplying by the rate according to the desired layer thickness. For the other material, the niobium layer is processed in the same way as the previous process, while the copper and niobium shutters for alloyed copper are simultaneously opened. The copper power is 100 W, while niobium is 19 W.
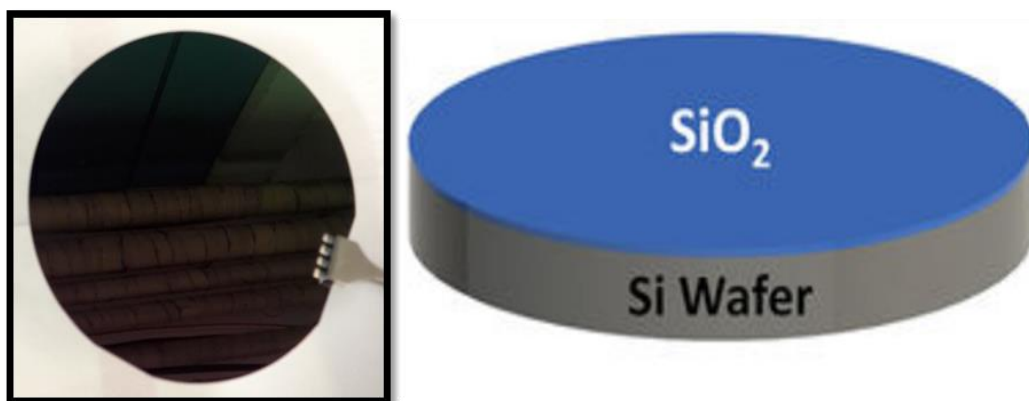
Figure 17. The image of the oxidized Si wafers.

Table 2 indicates the magnetron sputtering parameters. Base pressure indicates the pressure of the chamber before the coating starts. Coating pressure indicates the pressure in the chamber filled with inert gas. Argon flow rate is the rate of argon gas filling into the chamber and its unit is the Standard Cubic Centimeters per Minute (sccm).

Table 2. Magnetron Sputtering system parameters.

Base Pressure	1×10^{-7} Torr
Coating Pressure	2.3×10^{-3} Torr
Argon Flow Rate	50 sccm
Cu Rate(on RF)	11.9 nm/min
Nb Rate(on DC)	9.0 nm/min
Power RF and DC	100 W
Substrate	SiO_2 on Si

Before proceeding to the sample preparation, the deposition speed of the sputtering system per unit power was calibrated. Figure 18 gives a schematic illustration of the deposition geometry. The blue part shows the substrate to be coated. The yellow denotes the coating, and the coating is thicker in the regions closer to the gun.

Pure copper thin films with 1 μm thickness are coated at 100 W power to calibrate the deposition rate. Vacuum-compatible kapton tapes were used to create coated and shadowed regions on the substrate, which enabled measuring the thickness. 15 different points over three different lines were measured to calculate the deposition thickness. The thickness of each point was measured by a Dektak 3ST Surface Profilometer in Center for Solar Energy Research and Applications Center (GÜNAM). Each line scan was done over a length of 1 mm. Table 3 shows the results of the profilometry measurements.

The measurements showed a considerable difference in the coating thickness from the left side of the coating to the right side. This difference was about 20%, which can alter the layer thickness as well as the mechanical and microstructural properties. To avoid the uncertainties related to this, a small region of 5 mm x 5 mm was defined, and all the experiments were performed on this confined region. The thickness variation becomes less than 10% within the sample as a result of this precaution.

Table 3. The deposition rate for different materials for a gun power of 100 W.

Material	Thickness (nm)	Deposition Time (min)	Deposition Rate (nm/min)
Cu	1182	99	11.94
Nb	750	84	8.92
$Cu_{90}Nb_{10}$	1200	86	13.94
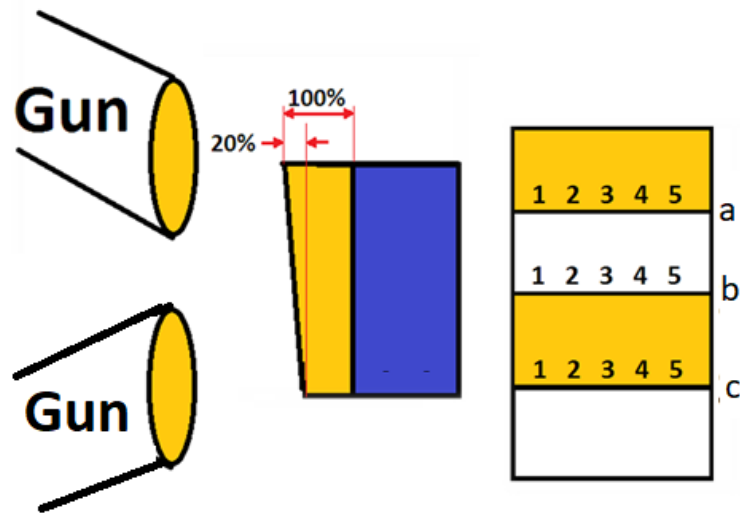
Figure 18. Top schematic view of the magnetron sputterer and measurement points used for calibration on the sample surface.
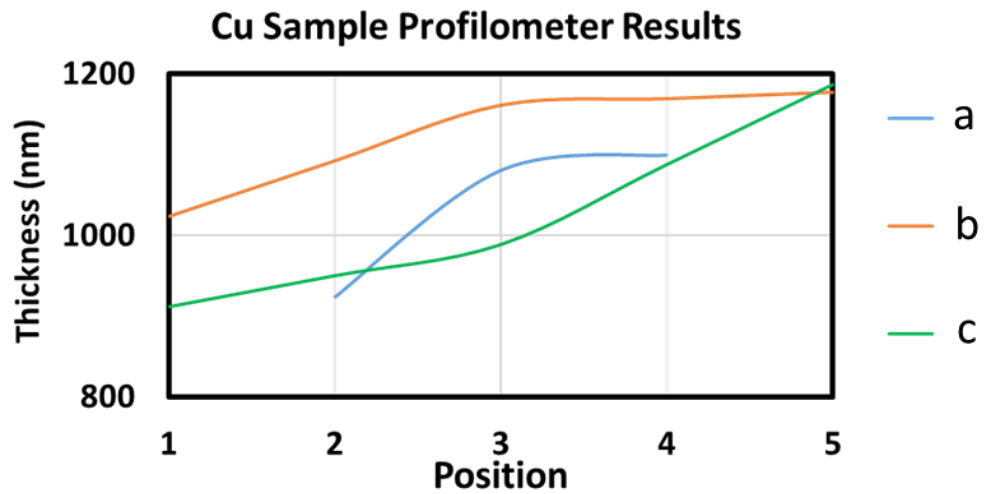
Figure 19. The results of deposition thickness measured by the profilometer.

2.2. Microstructural Characterization

Microstructural characterization is essential to relate the structural properties of materials to mechanical behavior. In this work, three main characterization methods were used. These are X-ray Diffraction (XRD), which gives information on crystal structure and grain sizes of materials, Scanning Electron Microscopy (SEM), which gives information about the sample surface, and Transmission Electron Microscopy (TEM), which provides more detailed information about the grain boundaries, dislocations, and interfaces.

2.2.1. X-Ray Diffraction and Grain Size Calculation

XRD measurements provide the crystallography and grain size of the specimens. In this technique, X-rays interact with the plane of atoms with a specific angle of incidence, theta. The instrument measures the intensity of the reflected beam, and angles of maximum intensity can be determined. Then Bragg's Law can be used to obtain the atomic spacing in between planes of atoms.

$$n\lambda = 2d_{hkl}sin\theta \tag{4}$$

Where d is the interatomic layer distance, λ is the wavelength of the incident X-ray beam, n is the diffraction order. hkl denotes the crystallographic plane of the sample.
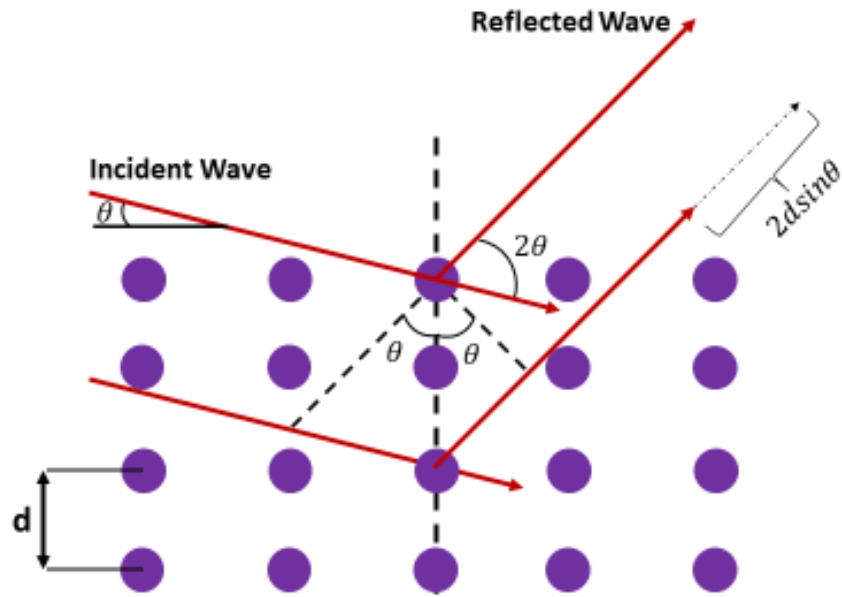
Figure 20. The schematic illustration of Bragg's Law [39]. The figure is taken from Ingham et. al. [39].

Analysis of XRD spectra also provides the grain size by using Scherrer Equation, which relates the peak width (*B*) and crystallite size (*L*):

$$B(2\theta) = \frac{K\lambda}{Lcos\theta} \tag{5}$$

Where *K* is the dimensionless value describing the shape factor and *B* is the full width of the associated diffraction peak at half maximum (*FWHM*). The value of *K* can be taken in the range 0.89 - 0.94 [39]. The expression dictates that, when the size of crystallite becomes smaller, the peak becomes wider. The detailed information can be found in the literature [40].

A Rigaku Ultima-IV diffractometer performed X-ray diffraction measurements on the samples in grazing incidence mode at 1°. Grain size was measured using the Scherrer equation by using Jade software. Copper wavelength ($K\alpha$) is 1.5418 A^0 , and the temperature is 296 K^0.

In many alloy systems, there is an upper concentration limit value, called the solubility limit, that atoms that are dissolved in a certain temperature can reach within the solving lattice. As you can see from Figure 21, you will see that the copper-niobium alloys are not solubility in the phase diagram. This means that Niobium actually does not dissolve in the Copper lattice. Therefore, although Cu and Nb are immiscible, we observe here solid solution form, due to the metastable condition created by the sputtering process.
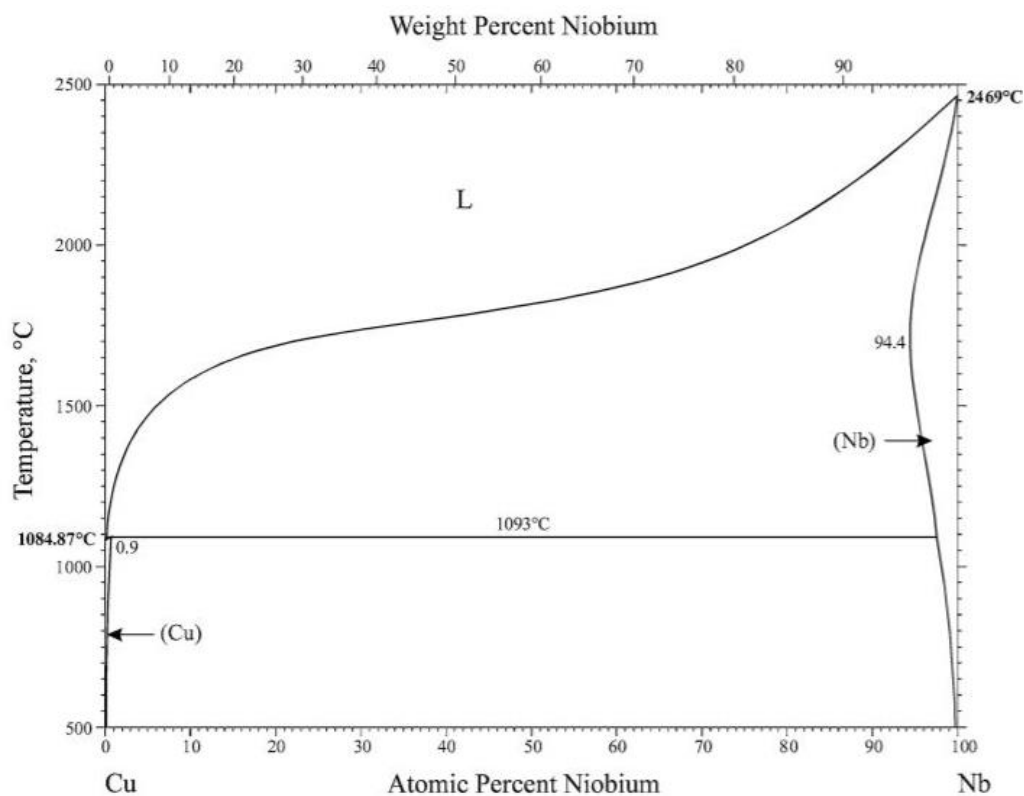
Figure 21. Cu/Nb phase diagram. This figure was taken from Okatoma [41]

2.2.2. Nanoindentation

All nanoindentation tests in this thesis were performed using an Agilent G200 nanoindenter equipped with a diamond Berkovich tip. The nanoindenter is located at Koç University Surface Science and Technology Center (KUYTAM). Nanoindentation tests were performed at room temperature and 15 different indentations were made in each sample for the repeatability of the experiment. These indents are at least 40 μm away from each other to minimize the influence from each other. Indentation locations were examined with the optical microscope of the nanoindenter, before performing the indentations, to minimize the effects of contamination such as dust particles and coating defects.

The continuous stiffness measurement method was used in these tests. One of the most important advantages of this method is that one can obtain the dynamic contact stiffness at every point on the loading curve. [42,43]. This provides a continuous property calculation as a function of depth into the surface, as opposed to a single value calculated for hardness and elastic modulus in the conventional hardness testing. Additionally, this method is less affected by artifacts such as thermal drift and mechanical drift. Figure 22 shows a hardness-depth curve that is obtained from the indentation of Cu/Nb 30 nm. In addition, Figure 23 shows a schematic of the cross-section of the indent.
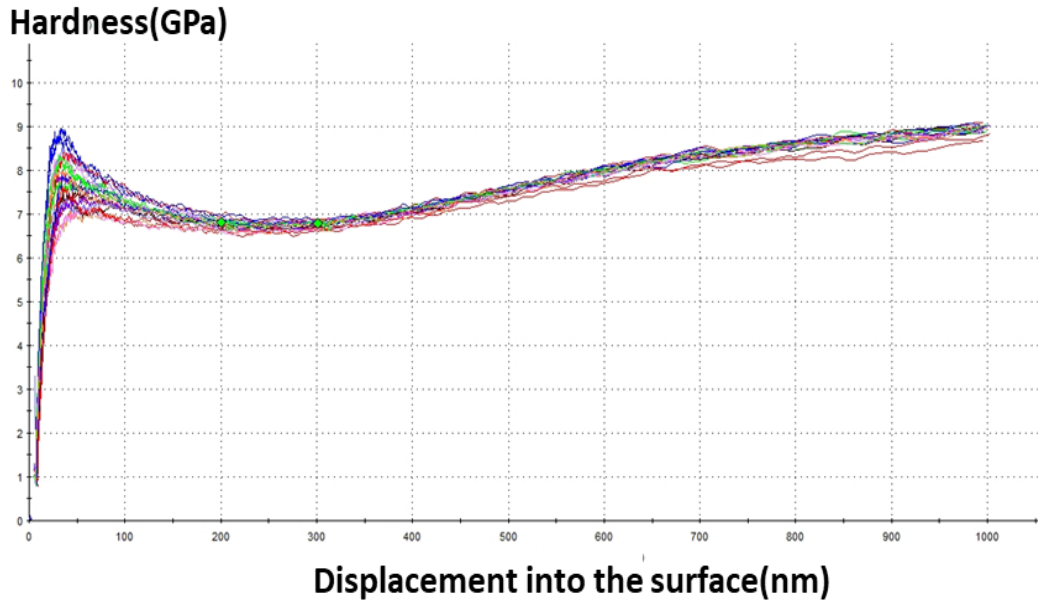
Figure 22. Hardness vs displacement curve of the nanoindentation test.
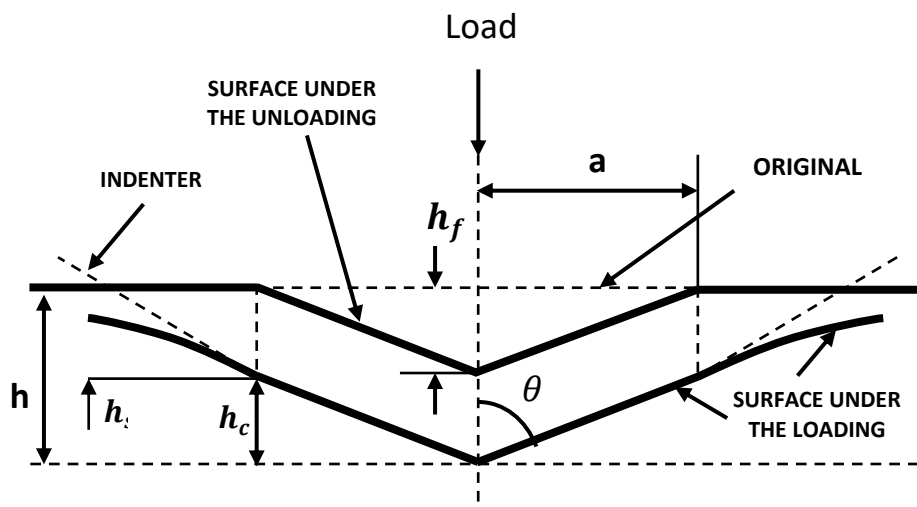
Figure 23. A Schematic illustration of an indentation section[25]. The figure is taken from Oliver et. al. [25].

The hardness of the sample can be determined by the following procedure. Indentation hardness is defined as:

$$H = \frac{P_{max}}{A_{projected}}$$

(6)

Where H is the hardness of the sample, P_{max} is maximum load, and A is the projected contact area between the indenter and the sample at maximum load. The maximum load is directly measured whereas the projected area requires calculation. The first step in the calculation is the determination of the contact stiffness (S). For this, the G200 nanoindenter uses the continuous stiffness measurements whose details are given by Li, et. al.[42].

Once S is determined then, the contact depth can be found as follows.

The total displacement h at any instant time during loading is described as:

$$h_{max} = h_c + h_s$$

(7)

where h_c is the contact depth and h_s is the displacement of the contact perimeter as shown in Figure 23. Then the relationship between the contact depth and h_s is as follows:

$$h_c = h_{max} - f_{inter} \frac{P_{max}}{S}$$

(8)

f_{inter} is a geometrical constant, and for a Berkovich tip, it is:

$$f_{inter} = \frac{2}{\pi}(\pi - 2) \tag{9}$$

Once h_c is determined, one can calculate the projected area as:

$$A = F(h_c) \tag{10}$$

For a Berkovich tip,

$$A_p = 24.5h_c^2 \tag{11}$$

This process outlined above is automatically performed by the Nanosuite software of the Agilent G200 nanoindenter.

2.2.3. Micropillar Compression

The micropillars were prepared by using a focused ion beam in Bilkent University, UNAM. Figure 24 shows a schematic of such systems. The dual-beam source consists of the two columns, a gallium ion source, and electron source. Gallium is preferred as the ion source material, as it has a low melting point (30 °C), which eases the operation of the ion source [34].
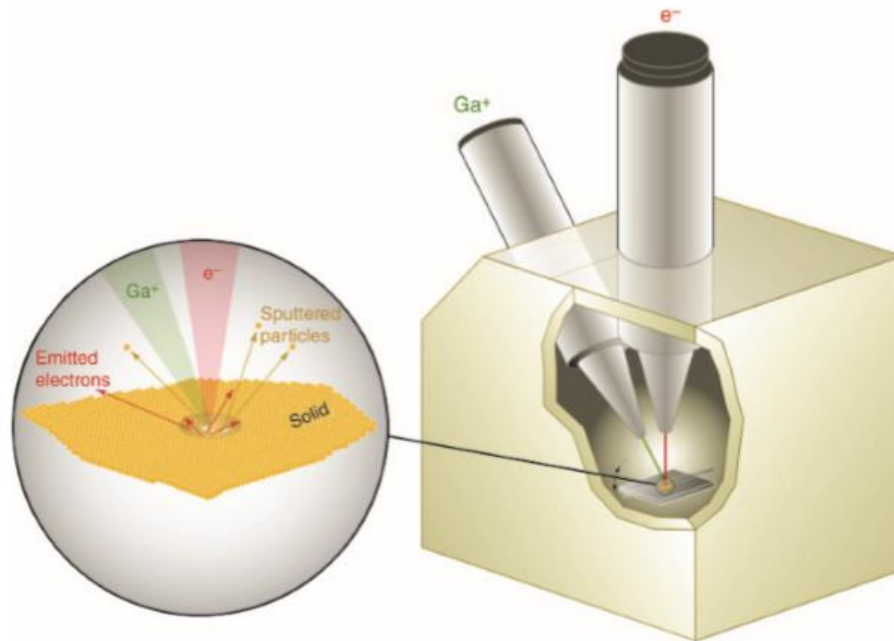
Figure 24. Schematic illustration of a dual-beam FIB-SEM instrument. The expanded view shows the electron and ion beam sample interaction [34]. The figure is taken from Volkert et. al. [34].

The ion column accelerates Ga to the solid surface, and upon contact with the specimen, the ion transfers its kinetic energy to the surface. As a result, the surface atoms are sputtered, and accurate control of the Ga beam enables the machining of precise features at the nanoscale [34].

Figure 25 shows pure copper micropillars prepared by the FEI Nova 600 Nanolab focused ion beam. First, an ion beam with a relatively high current of 6.3 nA milled a circular pattern of 25 μm outer diameter and 6 μm inner diameter. Machining of the micropillar was completed by gradually reducing the size of the milling pattern and the beam current, down to 100 pA.
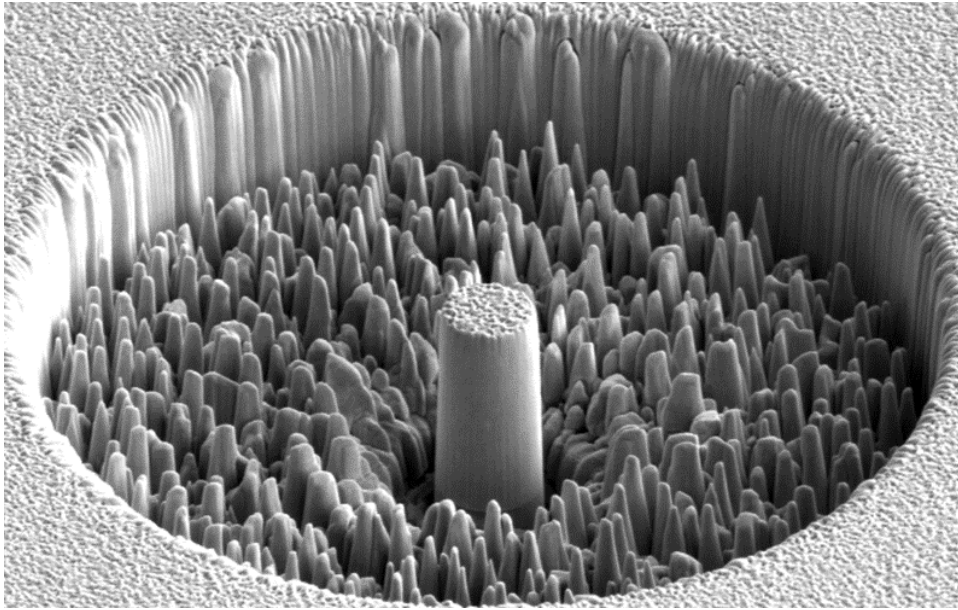
Figure 25. SEM image of pure copper micropillar.

CHAPTER 3

SOLID SOLUTION STRENGTHENING IN NANOLAYERED METAL

This chapter is reproduced with permission from *Alican Tuncay Alpkaya, Amir Motallebzadeh, Sezer Özerinç, Probing the mechanical behavior of nanostructured materials through micropillar compression experiments, Proceedings of the 19th International Metallurgy and Materials Congress, 2018, İstanbul, Turkey* [44] and *Alican Tuncay Alpkaya, Amir Motallebzadeh, Sezer Özerinç, Solid Solution Strengthening in Nanolayered Metals, Proceedings of the 13th Nanoscience and Nanotechnology Conference, 2017 , Antalya, Turkey* [45].

3.1. Introduction

Nanolayered metals are a new generation of nanomaterials composed of alternating layers of metals with layer thicknesses below 100 nm. These materials are promising for many engineering applications due to their high strength, good thermal stability and wear resistance [1]. The studies so far on these materials have focused on pure metal layers, and the effect of alloying additions on the strength is not well understood. This study aims to investigate the solid solution strengthening effects in Cu/Nb layers through Nb additions to the Cu layers.

3.2. Experimental details

1 μm-thick nanolayered films of Cu and Nb are magnetron sputtered on silicon substrates with layer thicknesses in the range 10 – 100 nm. The second set of samples were prepared with alternating $Cu_{90}Nb_{10}$ and Nb layers. X-ray diffraction

(XRD), scanning electron microscopy (SEM) and nanoindentation measurements characterized the microstructure and mechanical properties of the samples. Energy-dispersive X-ray spectroscopy verified the composition of the films. Further experimental details are provided in Chapter 2.

3.3. Microstructure

Figure 26 shows the SEM images of the cross sections of the Cu/Nb and $Cu_{90}Nb_{10}$ nanolayers. The images show that the layers are of uniform thickness with an alternating structure as desired. The alloyed nanolayers tend to be somewhat wavy in nature, but this is not expected to affect the mechanical properties drastically.
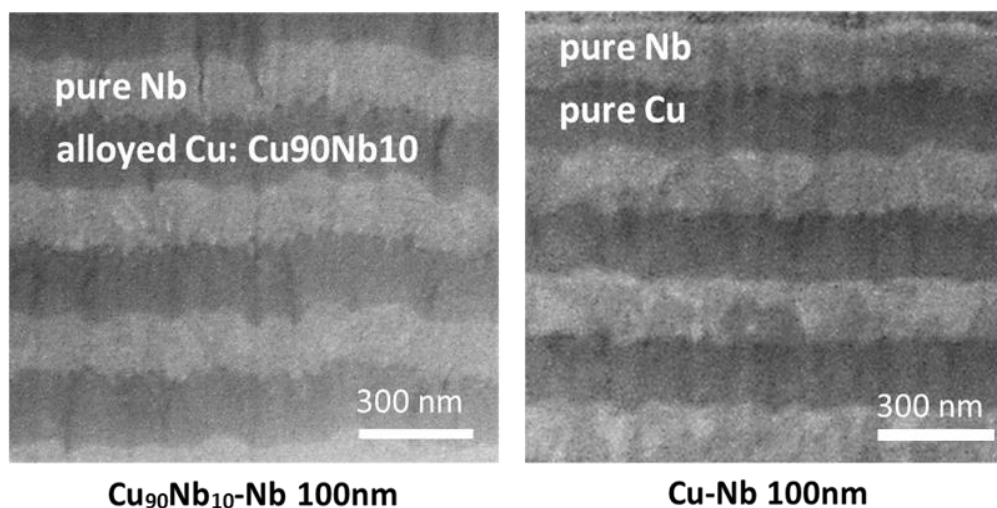
Figure 26. SEM images of the Cu/Nb and $Cu_{90}Nb_{10}$/Nb with 100 nm layer thickness.

Figure 27 shows the transmission electron microscopy (TEM) images of Cu/Nb multilayers in bright field mode. The nanocrystalline nature of the specimens is observed. The copper grains are mostly columnar in nature.
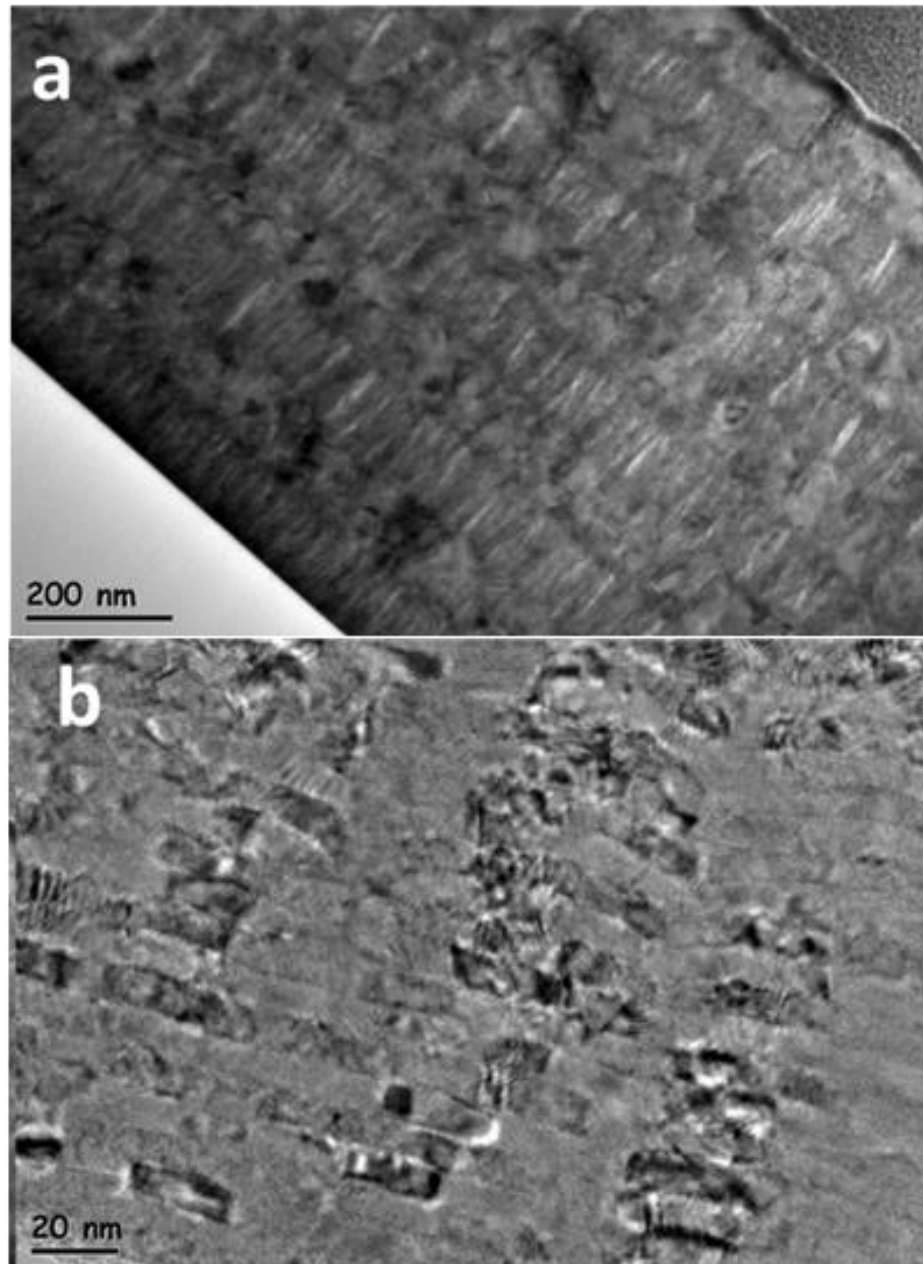
Figure 27. (a) Tem images of the Cu/Nb nanolayers with (a) 100 nm layer thickness (b) 10 nm layer thickness.

Figure 28 shows the X-ray diffraction data of pure Cu, monolithic $Cu_{90}Nb_{10}$, and multilayers. The nanolayered structure shows the peaks of both pure Cu and Nb,

verifying the purity of the layers. The $Cu_{90}Nb_{10}$/Nb multilayers show similar Cu peaks, indicating that the crystal structure of Cu is maintained in the alloyed layers. Copper atomic radius (128 pm) is smaller than niobium atomic radius (215 pm). The shifts of the Cu peaks towards smaller angles are due to the lattice distortion generated by the presence of large Nb solute atoms in the Cu lattice. Table 4 shows the grain sizes calculated by the Scherrer equation. Average grain size decreases with decreasing layer thickness and alloying additions also considerably decrease the grain size of Cu, especially for thick layers. For 10 nm layer thickness, this decrease seems negligible.
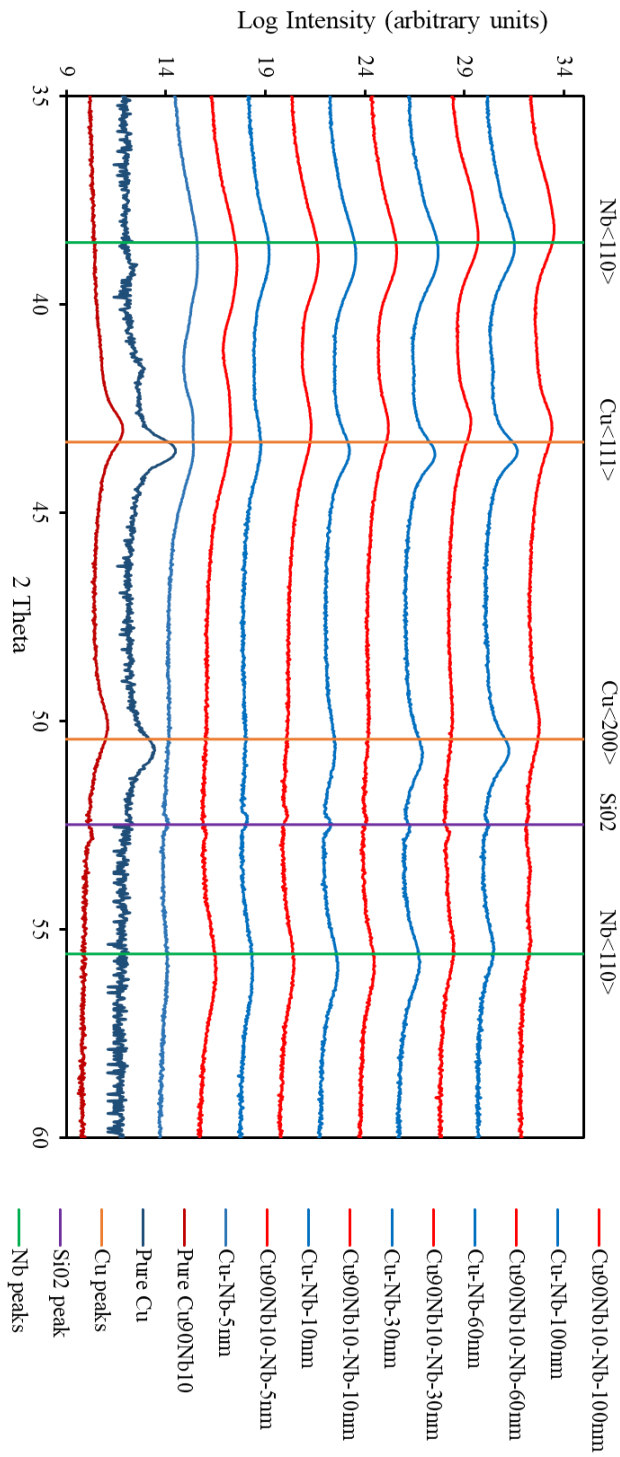
Figure 28. X-ray diffraction data of pure Cu, one layer Cu$_{90}$Nb$_{10}$, and multilayers.

Table 4. Average grain sizes of multilayers based on XRD data.

Layer Thickness (nm)	Sample	Nb Grain Size (nm)	Cu Grain Size (nm)
5	Cu/Nb	3.5	4.5
	$Cu_{90}Nb_{10}$/Nb	4	3.9
10	Cu/Nb	5.6	5.5
	$Cu_{90}Nb_{10}$/Nb	5.3	5.4
30	Cu/Nb	6.2	10.7
	$Cu_{90}Nb_{10}$/Nb	5.9	6.5
60	Cu/Nb	7.8	18
	$Cu_{90}Nb_{10}$/Nb	5.5	7.8
100	Cu/Nb	7.6	23.4
	$Cu_{90}Nb_{10}$/Nb	5.6	8.1
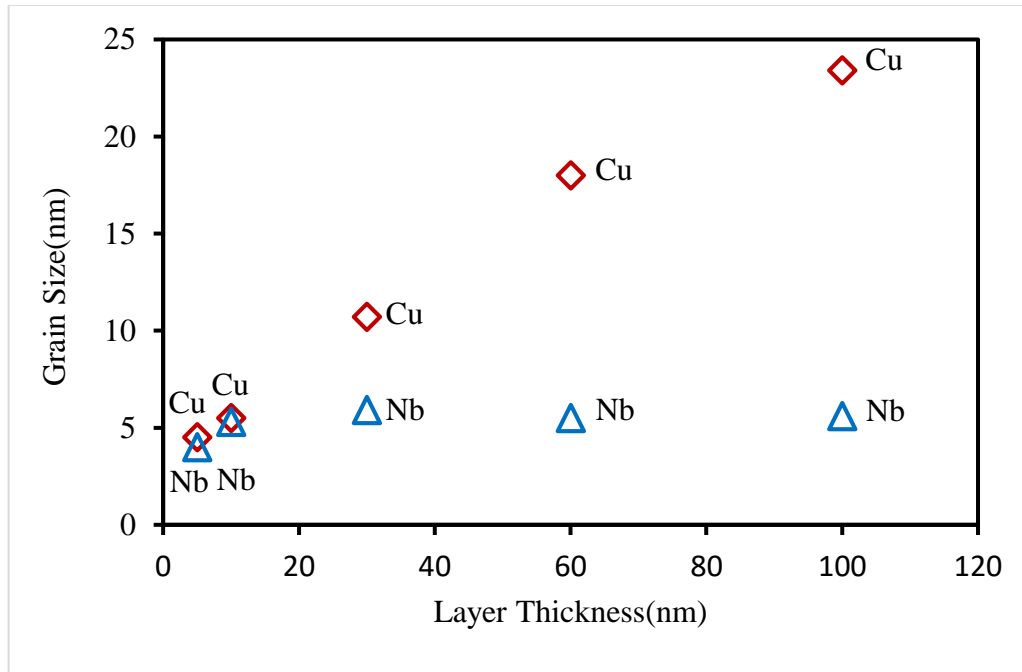
Figure 29. Grain size vs layer thickness for Cu/Nb nanolayered materials.
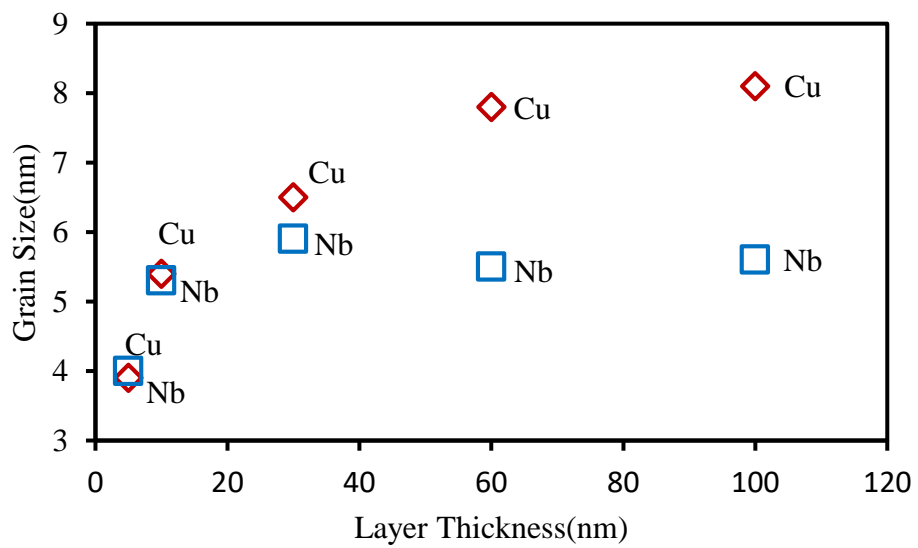
Figure 30. Grain size vs layer thickness for Cu90Nb10/Nb nanolayered materials.

3.4. Mechanical Properties

Figure 31 shows the hardness of all samples as a function of layer thickness. Cu/Nb values of the present study have good agreement with the previous data in the literature [46]. When it comes to the $Cu_{90}Nb_{10}$/Nb multilayers, a considerable increase in hardness is observed for all layer thicknesses.
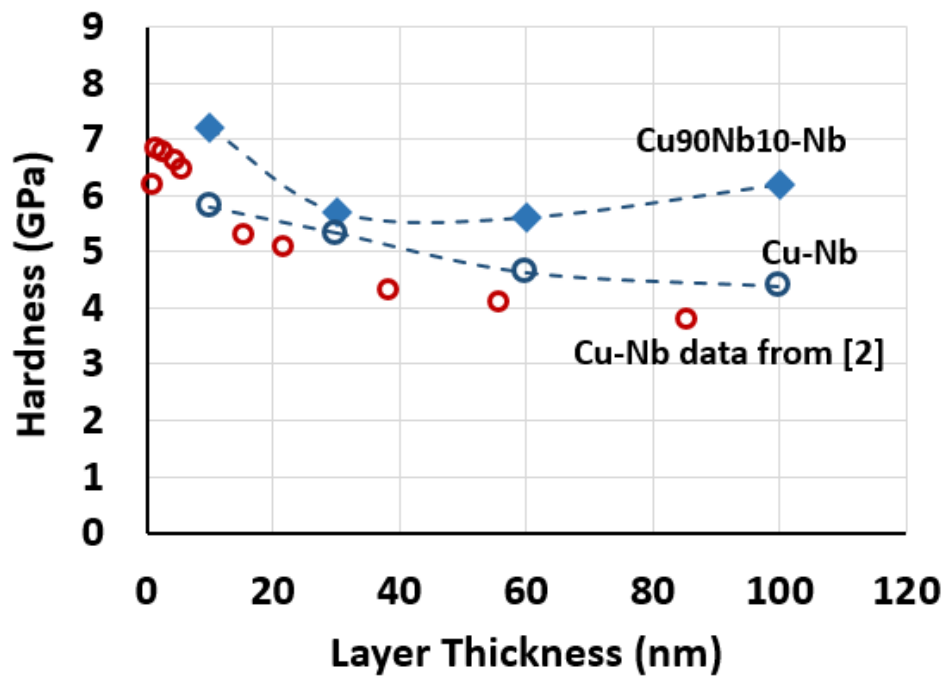
Figure 31. The hardness of multilayers of Cu/Nb and $Cu_{90}Nb_{10}$/Nb as a function of layer thickness. Literature values for Cu/Nb are shown for comparison [24].

3.5. Discussion

Both grain size variation and presence of Nb in solid solution form can affect the hardness. The grain sizes change at most by a factor of two by alloying additions and the associated Hall-Petch strengthening is not sufficient to explain the ≈1.5 GPa rise in hardness for 100 nm layers [47,48]. On the other hand, previous studies have shown that small alloying additions can improve the strength of nanocrystalline copper considerably, through a decrease in grain boundary energy [49]. For example, Figure 32 shows the hardness enhancement as a result of Nb additions to monolithic films of nanocrystalline copper [50].
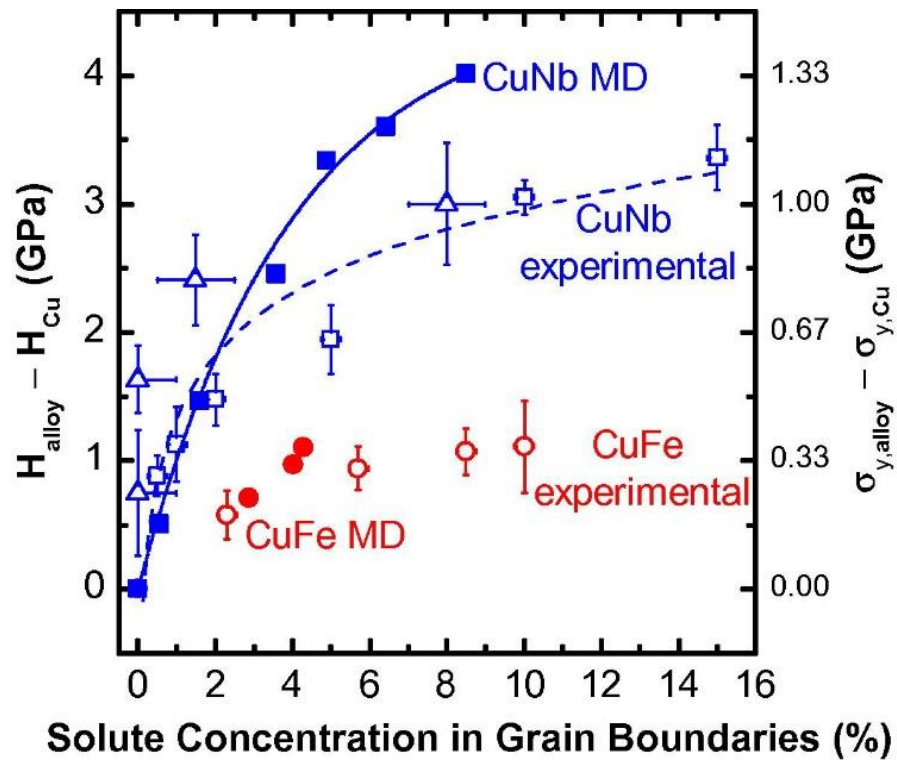
Figure 32. Hardness enhancement obtained by adding Nb or Fe to Cu when compared to pure Cu as a function of grain boundary solute concentration. The figure is taken from Özerinç et. al. [50].

43

In order to gain further insight into the results, Table 5 and Figure 33 summarize the hardness enhancement observed in nanolayers as a function of layer thickness. Starting from 100 nm down to 30 nm layer thickness, the hardness enhancement monotonically decreases. Another parameter that changes over this regime is the ratio of the grain boundary volume to that of interface volume. For example, for a layer thickness of 100 nm, the grain sizes are 18 and 10 nm for the pure and alloyed Cu layers, whereas, for a layer thickness of 30, these values are 11 and 6, respectively. Therefore, there are about 5-10 grains over a layer for 100 nm layers whereas this number reduces to 3-5 for 30 nm. As a result, interface volume starts to increase when compared to grain boundary volume and the effect of grain boundary plasticity on strength gradually becomes less important. Since the alloying additions significantly affect the grain boundary energy but not the interfacial strength, this implies a decrease in hardness enhancement with decreasing layer thickness, as observed in the data.

When it comes to a layer thickness of 10 and 5 nm, there are indications of a different regime of plasticity, where now the enhancement increases when compared to 30 nm layers. This requires further investigation, as for this layer thickness, grain boundaries are no longer dominant, and the alloying additions might increase the grain boundary thickness, which is not a big effect for 100 nm nanolayers but it is a considerable change for very thin layers. This trend observed for 5 and 10 nm layers require further investigation through high-resolution transmission electron microscopy, which will be part of the future work.

Table 5. Summary of hardness values with respect to layer thickness.

Layer Thickness (nm)	Hardness (GPa)		
	Cu/Nb	$Cu_{90}Nb_{10}$/Nb	Enhancement
5	6.24	6.98	0.74
10	5.64	6.74	1.1
30	5.08	5.42	0.34
60	4.45	5.47	1.02
100	4.38	6.01	1.63
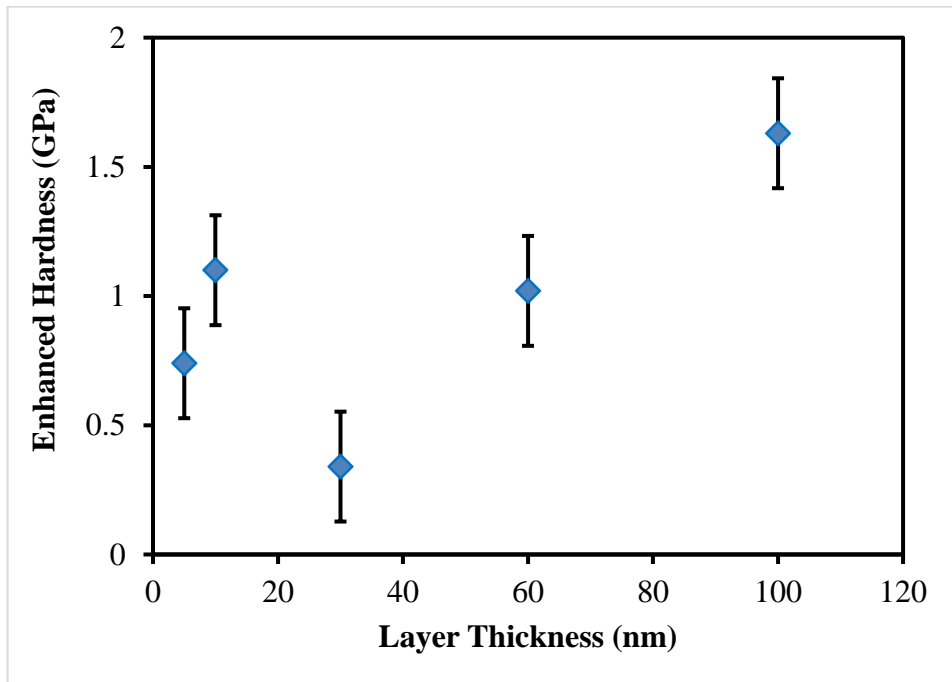
Figure 33. Enhanced hardness vs layer thickness.

3.6. Conclusions

We demonstrated considerable strengthening in metallic multilayers of Cu/Nb through alloying additions. The hardness of the 10 nm Cu90Nb10/Nb film is higher than the strongest Cu/Nb multilayer previously produced. Alloying additions to the softer layers in nanolayered metals offer an effective approach to the optimization of the strength of nanostructured materials.

CHAPTER 4

CONCLUSIONS

In this dissertation, the effects of layer thickness and alloying additions on the mechanical properties of Cu/Nb and alloyed Cu/Nb nanolayered materials were investigated. For these purposes, pure and alloyed Cu/Nb nanolayered materials with layer thicknesses varying from 5 nm to 100 nm were produced by magnetron sputtering. Nanoindentation and micropillar compression tests were performed to investigate the mechanical properties of these materials.

The results showed that hardness increases with decreasing layer thickness, in agreement with previous findings in the literature. In addition, alloying additions strengthen the nanolayers considerably. This strengthening decreases as the layer spacing is varied from 100 nm to 30 nm, due to the diminishing effect of grain boundary strengthening and increasing effect of interface strengthening. On the other hand, there is a secondary trend of increasing hardening for 5 and 10 nm layers, which requires further investigation. It should also be noted that the hardness of 5 nm Cu90Nb10/Nb film is higher than the strongest Cu/Nb multilayer previously produced.

This thesis provided experimental evidence that alloying additions offer an effective way of optimizing the strength of nanocrystalline materials.

4.1. Preliminary Results of Micropillar Compression

In this section, preliminary results of micropillar compression experiments are presented and future work regarding these experiments are summarized.

Pure nanocrystalline Cu films were deposited on oxidized single crystal silicon substrates by means of magnetron sputtering. The base pressure in the chamber prior to sputtering was 1×10^{-7} Torr and Ar pressure during sputtering was 2.3×10^{-3} Torr. Cu deposition rate was 17 nm/s. The total film thickness was about $6 \ \mu m$.

An FEI Nova 600 Nanolab focused ion beam fabricated the micropillars. Ga+ ions sputtered away from the material locally in the desired geometry. First, an ion beam with a relatively high current of 6.3 nA milled a circular pattern of 25 µm outer diameter and 6 µm inner diameter. Machining of the micropillar was completed by gradually reducing the size of the milling pattern and the beam current, down to 100 pA. The Agilent G200 nanoindenter compressed the micropillars at a constant displacement rate of 3 nm/s using a 10 µm diameter flat diamond punch.

Figure 34 shows a nanocrystalline Cu micropillar prepared by the focused ion beam, before and after testing.
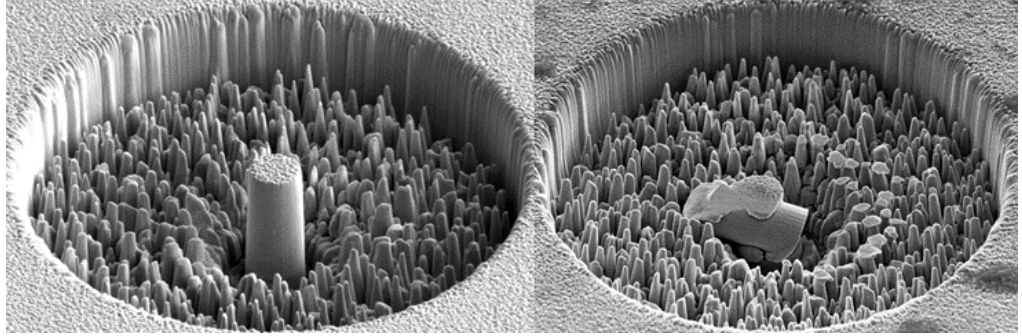
Figure 34. The SEM image of the pure copper pillar (before compression and after compression).
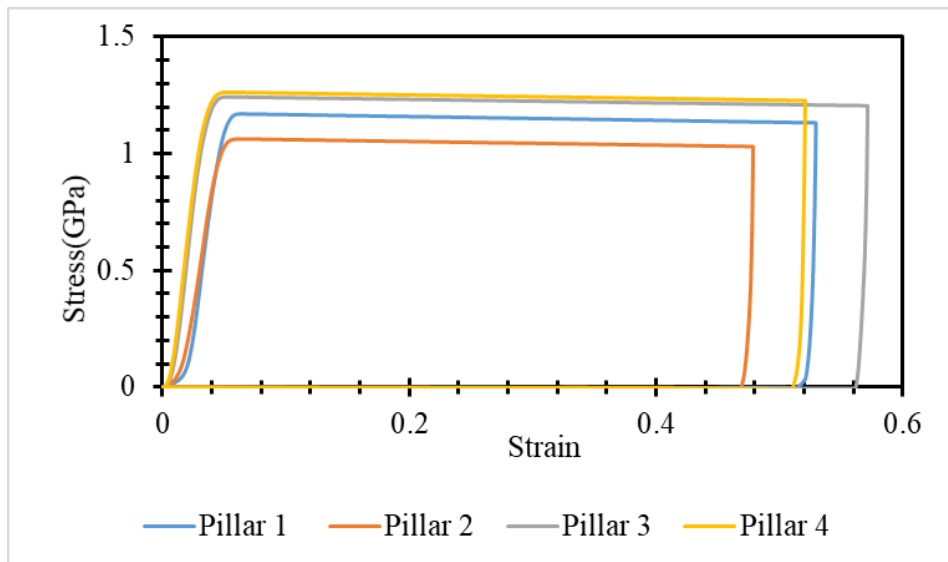
Figure 35. Stress-strain behavior of the pure copper nanocrystalline material.

Figure 35 shows the stress-strain behavior of the compressed micropillars. These are somewhat low values for nanocrystalline copper, and the post-testing SEM images indicate that the micropillar mostly bends, instead of the desired uniaxial

compression scheme. Therefore, further efforts will be necessary to optimize the compression experiments.

In this dissertation, micropillar compression tests conducted on pure copper and Cu / Nb multilayer metals are in agreement with the literature, which is promising for further study on this subject. However, we will do more testing to ensure the experimental improvement such as layers with better adherence, to minimize taper angle of the pillar and to produce more pillars with perfect geometry that are most favorable in micropillar experiments. After we have provided these experimental improvements, we will perform tests on alloyed Cu/Nb multilayers with different layer thicknesses. Then, by comparing the micro-compression test results with the indentation results, we will contribute to the study of alloyed Cu/Nb metallic multilayer which is missing in the literature.

4.2. Future Work

One of the future work paths is investigating the effect of different levels of niobium addition into the copper lattice on the mechanical properties. It will also be performed successful pillar compression experiments to directly probe the mechanical properties of nanostructured materials. For this purpose, the produced micropillars should be perfectly geometry and the pillar should not tumble when the punch applies to force on the pillars so that there will be uniaxial compression instead of the bending force occurring in the pillar.

Additionally, the micro-compression tests will be related to the investigation of the mechanical properties of nanolayered metals upon alloying additions, whose effects on mechanical properties are currently not known. Then, the nanolayered micropillars will be tested and the yield strength determined directly instead of hardness.

On the other hand, it should be understood the relationship between grain size, layer thickness, and strength. For this purpose, it is necessary to do more experiments such as SEM, TEM which perform atomic-scale imaging. Thus, these experiments enable the understanding of the nanostructure deformation mechanisms.

CHAPTER 5

REFERENCES

[1] A.H. Chokshi, A. Rosen, J. Karch, H. Gleiter, On the validity of the hall-petch relationship in nanocrystalline materials, Scr. Metall. 23 (1989) 1679–1683. doi:10.1016/0036-9748(89)90342-6.

[2] D. Jang, X. Li, H. Gao, J.R. Greer, Deformation mechanisms in nanotwinned metal nanopillars, Nat. Nanotechnol. 7 (2012) 594–601. doi:10.1038/nnano.2012.116.

[3] J. Wang, A. Misra, An overview of interface-dominated deformation mechanisms in metallic multilayers, Curr. Opin. Solid State Mater. Sci. 15 (2011) 20–28. doi:10.1016/j.cossms.2010.09.002.

[4] S. Özerinç, K. Tai, N.Q. Vo, P. Bellon, R.S. Averback, W.P. King, Grain boundary doping strengthens nanocrystalline copper alloys, Scr. Mater. 67 (2012) 720–723. doi:10.1016/j.scriptamat.2012.06.031.

[5] T.J. Rupert, J.C. Trenkle, C.A. Schuh, Enhanced solid solution effects on the strength of nanocrystalline alloys, Acta Mater. 59 (2011) 1619–1631. doi:10.1016/j.actamat.2010.11.026.

[6] A. Misra, R.G. Hoagland, H. Kung ‡, Thermal stability of self-supported nanolayered Cu/Nb films, Philos. Mag. 84 (2004) 1021–1028. doi:10.1080/14786430310001659480.

[7]   M.J. Demkowicz, P. Bellon, B.D. Wirth, Atomic-scale design of radiation-tolerant nanocomposites, MRS Bull. 35 (2010) 992–998. doi:10.1557/mrs2010.704.

[8]   E.O. Hall, Yield Point Phenomena in Metals and Alloys, Springer US, Boston, MA, 1970. doi:10.1007/978-1-4684-1860-6.

[9]   J. R. Weertman, Hall-Petch strengthening in nanocrystalline metals, Mater. Sci. Eng. A166 (1993) 161–167.

[10]   V.G. Gryaznov, M.Y. Gutkin, A.E. Romanov, L.I. Trusov, On the yield stress of nanocrystals, J. Mater. Sci. 28 (1993) 4359–4365. doi:10.1007/BF01154943.

[11]   T.G. Nieh, J. Wadsworth, Hall-Petch Relation in Nanocrystalline Solids, Scr. Metall. (1991) 955–958.

[12]   A. Misra, M.J. Demkowicz, J. Wang, R.G. Hoagland, The multiscale modeling of plastic deformation in metallic nanolayered composites, JOM. 60 (2008) 39–42. doi:10.1007/s11837-008-0047-6.

[13]   K. Lu, W.D. Wei, Microhardness and Fracture Properties of Nanocrystalline Ni-P Alloys, Scr. Metall. 24 (1990) 2319–2323.

[14]   S.S. Quek, Z.H. Chooi, Z. Wu, Y.W. Zhang, D.J. Srolovitz, The inverse hall–petch relation in nanocrystalline metals: A discrete dislocation dynamics analysis, J. Mech. Phys. Solids. 88 (2016) 252–266. doi:10.1016/j.jmps.2015.12.012.

[15]   C.E. Carlton, P.J. Ferreira, What is behind the inverse Hall–Petch effect in nanocrystalline materials?, Acta Mater. 55 (2007) 3749–3756. doi:10.1016/j.actamat.2007.02.021.

[16] A. Misra, J.P. Hirth, R.G. Hoagland, Length-scale-dependent deformation mechanisms in incoherent metallic multilayered composites, Acta Mater. 53 (2005) 4817–4824.

[17] J.-H. Xu, T. Oguchi, A.J. Freeman, Solid-solution strengthening: Substitution of V in Ni 3 Al and structural stability of Ni 3 (Al,V), Phys. Rev. B. 36 (1987) 4186–4189. doi:10.1103/PhysRevB.36.4186.

[18] D.M. Dimiduk, M.D. Uchic, T.A. Parthasarathy, Size-affected single-slip behavior of pure nickel microcrystals, Acta Mater. 53 (2005) 4065–4077. doi:10.1016/j.actamat.2005.05.023.

[19] A.T. Jennings, M.J. Burek, J.R. Greer, Microstructure versus Size: Mechanical Properties of Electroplated Single Crystalline Cu Nanopillars, Phys. Rev. Lett. 104 (2010). doi:10.1103/PhysRevLett.104.135503.

[20] A. Misra, M.J. Demkowicz, X. Zhang, R.G. Hoagland, The radiation damage tolerance of ultra-high strength nanolayered composites, JOM. 59 (2007) 62–65. doi:10.1007/s11837-007-0120-6.

[21] I.J. Beyerlein, N.A. Mara, J.S. Carpenter, T. Nizolek, W.M. Mook, T.A. Wynn, R.J. McCabe, J.R. Mayeur, K. Kang, S. Zheng, J. Wang, T.M. Pollock, Interface-driven microstructure development and ultra-high strength of bulk nanostructured Cu-Nb multilayers fabricated by severe plastic deformation, J. Mater. Res. 28 (2013) 1799–1812. doi:10.1557/jmr.2013.21.

[22] I. J. Beyerlein, N. A. Mara,et al., Structure–Property–Functionality of Bimetal Interfaces, JOM. Vol. 64 (2012) 1192–1207.

[23] J. Wang, Q. Zhou, S. Shao, A. Misra, Strength and plasticity of nanolaminated materials, Mater. Res. Lett. 5 (2017) 1–19. doi:10.1080/21663831.2016.1225321.

[24] C.A. Schuh, Nanoindentation studies of materials, Mater. Today. 9 (2006) 32–40. doi:10.1016/S1369-7021(06)71495-X.

[25] W.C. Oliver, G.M. Pharr, An improved technique for determining hardness and elastic modulus using load and displacement sensing indentation experiments, J. Mater. Res. 7 (1992) 1564–1583. doi:10.1557/JMR.1992.1564.

[26] B. Bhushan, ed., Handbook of micro/nanotribology, 2nd ed, CRC Press, Boca Raton, 1999.

[27] J.R. CAHOON, W.H. BROUGHTON, A.R. KUTZAK, The determination of yield strength from hardness measurements, Metall. Trans. (n.d.) 5.

[28] T.Y. Tsui, J. Vlassak, W.D. Nix, Indentation plastic displacement field: Part II. The case of hard films on soft substrates, J. Mater. Res. 14 (1999) 2204–2209. doi:10.1557/JMR.1999.0296.

[29] C. Gamonpilas, E.P. Busso, On the effect of substrate properties on the indentation behaviour of coated systems, Mater. Sci. Eng. A. 380 (2004) 52–61. doi:10.1016/j.msea.2004.04.038.

[30] S. Chen, L. Liu, T. Wang, Investigation of the mechanical properties of thin films by nanoindentation, considering the effects of thickness and different coating–substrate combinations, Surf. Coat. Technol. 191 (2005) 25–32. doi:10.1016/j.surfcoat.2004.03.037.

[31] F. Cleymand, O. Ferry, R. Kouitat, A. Billard, J. von Stebut, Influence of indentation depth on the determination of the apparent Young's modulus of bi-layer material: Experiments and numerical simulation, Surf. Coat. Technol. 200 (2005) 890–893. doi:10.1016/j.surfcoat.2005.02.086.

[32] J. Hay, B. Crawford, Measuring substrate-independent modulus of thin films, J. Mater. Res. 26 (2011) 727–738. doi:10.1557/jmr.2011.8.

[33] H. Zhang, B.E. Schuster, Q. Wei, K.T. Ramesh, The design of accurate micro-compression experiments, Scr. Mater. 54 (2006) 181–186. doi:10.1016/j.scriptamat.2005.06.043.

[34] C.A. Volkert, A.M. Minor, Focused Ion Beam Microscopy and Micromachining, MRS Bull. 32 (2007) 389–399. doi:10.1557/mrs2007.62.

[35] N.A. Mara, D. Bhattacharyya, P.O. Dickerson, R.G. Hoagland, A. Misra, Ultrahigh Strength and Ductility of Cu-Nb Nanolayered Composites, Mater. Sci. Forum. 633–634 (2009) 647–653. doi:10.4028/www.scientific.net/MSF.633-634.647.

[36] D.M. Mattox, Handbook of physical vapor deposition (PVD) processing, 2. ed, Elsevier, Amsterdam, 2010.

[37] P.. Kelly, R.. Arnell, Magnetron sputtering: a review of recent developments and applications, Vacuum. 56 (2000) 159–172. doi:10.1016/S0042-207X(99)00189-X.

[38] A. Misra, M. Verdier, Y.. Lu, H. Kung, T.. Mitchell, M. Nastasi, J.. Embury, Structure and mechanical properties of Cu-X (X = Nb,Cr,Ni) nanolayered composites, Scr. Mater. 39 (1998) 555–560. doi:10.1016/S1359-6462(98)00196-1.

[39] B. Ingham, M.F. Toney, X-ray diffraction for characterizing metallic films, in: Met. Films Electron. Opt. Magn. Appl., Elsevier, 2014: pp. 3–38. doi:10.1533/9780857096296.1.3.

[40] J.I. LANGFORD, A.J.C. WILSON, Seherrer after Sixty Years: A Survey and Some New Results in the Determination of Crystallite Size, (n.d.) 12.

[41] H. Okamoto, Section III: Supplemental Literature Review, J. Phase Equilibria. 19 (1998) 486–486. doi:10.1007/BF02700865.

[42] X. Li, B. Bhushan, A review of nanoindentation continuous stiffness measurement technique and its applications, Mater. Charact. 48 (2002) 11–36. doi:10.1016/S1044-5803(02)00192-4.

[43] T. Wen, J. Gong, Z. Peng, D. Jiang, C. Wang, Z. Fu, H. Miao, Analysis of continuous stiffness data measured during nanoindentation of titanium films on glass substrate, Mater. Chem. Phys. 125 (2011) 500–504. doi:10.1016/j.matchemphys.2010.10.026.

[44] Alican Tuncay Alpkaya, Amir Motallebzadeh, Sezer Özerinç, Probing the mechanical behavior of nanostructured materials through micropillar compression experiments, 19th Int. Metall. Mater. Congr. (2018).

[45] Alican T. Alpkaya, Amir Motallebzadeh, Sezer Özerinç, Solid Solution Strengthening in Nanolayered Metals, in: Turkey, 2017.

[46] T. Nizolek, N.A. Mara, I.J. Beyerlein, J.T. Avallone, J.E. Scott, T.M. Pollock, Processing and Deformation Behavior of Bulk Cu–Nb Nanolaminates, Metallogr. Microstruct. Anal. 3 (2014) 470–476. doi:10.1007/s13632-014-0172-2.

[47] J. Chen, L. Lu, K. Lu, Hardness and strain rate sensitivity of nanocrystalline Cu, Scr. Mater. 54 (2006) 1913–1918. doi:10.1016/j.scriptamat.2006.02.022.

[48] K.M. Youssef, R.O. Scattergood, K.L. Murty, J.A. Horton, C.C. Koch, Ultrahigh strength and high ductility of bulk nanocrystalline copper, Appl. Phys. Lett. 87 (2005) 091904. doi:10.1063/1.2034122.

[49] G.M. Pharr, A. Bolshakov, Understanding nanoindentation unloading curves, J. Mater. Res. 17 (2002) 2660–2671. doi:10.1557/JMR.2002.0386.

[50] S. Özerinç, K. Tai, N.Q. Vo, P. Bellon, R.S. Averback, W.P. King, Grain boundary doping strengthens nanocrystalline copper alloys, Scr. Mater. 67 (2012) 720–723. doi:10.1016/j.scriptamat.2012.06.031.